Available online at www.sciencedirect.com
ScienceDirect
Geochimica et Cosmochimica Acta 73 (2009) 7360–7386
Geochimica et Cosmochimica Acta
www.elsevier.com/locate/gca

Evidence for high-pressure core-mantle differentiation from the metal–silicate partitioning of lithophile and weakly-siderophile elements

Ute Mann *, Daniel J. Frost, David C. Rubie

Bayerisches Geoinstitut, University of Bayreuth, D-95440 Bayreuth, Germany

Received 16 January 2009; accepted in revised form 5 August 2009; available online 19 August 2009

Abstract

Liquid Fe metal–liquid silicate partition coefficients for the lithophile and weakly-siderophile elements Ta, Nb, V, Cr, Si, Mn, Ga, In and Zn have been measured in multianvil experiments performed from 2 to 24 GPa, 2023–2873 K and at oxygen fugacities of −1.3 to −4.2 log units relative to the iron-wüstite buffer. Compositional effects of light elements dissolved in the metal liquid (S, C) have been examined and experiments were performed in both graphite and MgO capsules, specifically to address the effect of C solubility in Fe-metal on siderophile element partitioning. The results were used to examine whether there is categorical evidence that a significant portion of metal–silicate equilibration occurred under very high pressures during core-mantle fractionation on Earth. Although the depletion of V from the mantle due to core formation is significantly greater than that of Nb, our results indicate that both elements have similar siderophile tendencies under reducing conditions at low pressures. With increasing pressure, however, Nb becomes less siderophile than V, implying that average metal–silicate equilibration pressures of at least 10–40 GPa are required to explain the Nb/V ratio of the mantle. Similarly the moderately-siderophile, volatile element ratios Ga/Mn and In/Zn are chondritic in the mantle but both volatility and core-mantle equilibration at low pressure would render these ratios strongly sub-chondritic. Our results indicate that pressures of metal–silicate partitioning exceeding 30–60 GPa would be required to render these element ratios chondritic in the mantle. These observations strongly indicate that metal–silicate equilibration must have occurred at high pressures, and therefore support core-formation models that involve deep magma oceans. Moreover, our results allow us to exclude models that envisage primarily low-pressure (<1 GPa) equilibration in relatively small planetary bodies. We also argue that the core cannot contain significant U as this would require metal–silicate equilibration at oxygen fugacities low enough for significant amounts of Ta to have also been extracted from the mantle. Likewise, as In is more siderophile than Pb but similarly volatile and also quite chalcophile it would have been difficult for Pb to enter the core without reversing the relative depletions of these elements in the mantle unless metal–silicate equilibration occurred at high pressures >20 GPa.

1. INTRODUCTION

One of the most important differentiation events in Earth's history was the formation of its Fe-rich core by the physical separation of metal from the silicate mantle. Most of the constraints on how this differentiation event occurred are based on the comparison between the geochemistry of the Earth's mantle and chondritic meteorites. Any successful model for core formation must identify conditions under which element partitioning, together with other processes, would have established the present-day element abundance pattern of the Earth's mantle (Fig. 1). The ratios of refractory lithophile elements in the Earth's mantle indicate that the Earth accreted from material that was chemically similar to chondritic meteorites (McDonough and Sun, 1995; O'Neill and Palme, 1998; Palme and O'Neill, 2003). During core-mantle differentiation, the partitioning

* Corresponding author. Present address: ETH Zürich, Institut für Mineralogie und Petrographie, Sonneggstrasse 5, CH-8092 Zürich, Switzerland. Tel.: +41 44 63 236 91; fax: +41 44 632 16 36.
E-mail address: ute.mann@erdw.ethz.ch (U. Mann).

0016-7037/$ - see front matter © 2009 Elsevier Ltd. All rights reserved.
doi:10.1016/j.gca.2009.08.006

of elements between metal and silicate resulted in the depletion of siderophile (metal-loving) elements in the mantle because of their strong affinities for metal. However, it has been known for many years that the mantle contains considerably higher concentrations of siderophile elements than are predicted by partitioning experiments performed at 1 bar and temperatures of 1473–1673 K (Ringwood, 1979; Newsom, 1990; Walter et al., 2000). Explaining this 'excess siderophile element problem' forms the basis for understanding core formation in the Earth.

One of the first solutions was proposed by Wänke (1981) with the following heterogeneous 2-stage accretion model: During the first stage of Earth's formation, small bodies accreted from volatile-poor, reduced material with metal–silicate equilibration occurring at low pressures (e.g. <1 GPa). As a result of the reducing conditions, all elements more siderophile than Fe were completely extracted from the silicate mantles and weakly-siderophile elements such as V, Cr, Mn and Si were also partly extracted into the cores of these bodies. These small differentiated objects subsequently accreted to form larger bodies, with the metallic cores merging without any re-equilibration of metal and silicate. In a second stage, oxidised, CI-like material nearly free of Fe metal was accreted such that no further core formation occurred. Through the mixing of this material into the previously-depleted mantle of the proto-Earth, the siderophile element abundances of the mantle were established, with elements such as Ni, Co and W being present in chondritic relative proportions. O'Neill (1991) further developed this low-pressure core-formation model in order to explain the highly-siderophile element abundances in the mantle (Fig. 1). These heterogeneous accretion models successfully explained the current mantle concentrations of many siderophile elements with an essential feature being metal–silicate equilibration at low pressures (e.g. <1 GPa).

With data from high-pressure experiments becoming available, it was discovered that Ni and Co become less siderophile with increasing pressure. Consequently it was proposed in the mid-1990's that the high concentrations of Ni and Co in the mantle together with their chondritic ratio can be explained by metal–silicate equilibration at pressures of e.g. 20–60 GPa in a deep terrestrial magma ocean (Li and Agee, 1996, 2001; Righter et al., 1997; O'Neill et al., 1998; Rubie et al., 2003; Chabot et al., 2005). High-pressure core-formation models have since been extended to include other elements (e.g. Gessmann and Rubie, 2000; Chabot and Agee, 2003). Wade and Wood (2005) developed a model of continuous core formation in which the pressure of metal–silicate equilibration increased to ~60 GPa as the planet grew by the addition of impactor material. In particular, they showed that the oxygen fugacity would have to be initially low but would have to increase significantly during accretion in order to explain the mantle abundances of Fe and weakly-siderophile elements such as Si, V and Mn (see also Corgne et al., 2008; Wood et al., 2008b).

Core-formation models based on high-pressure metal–silicate equilibration have become popular in recent years, but both the low- and high-pressure models summarised above appear able to explain the mantle depletions of a large number of moderately- and weakly-siderophile elements although both types of model entail significant uncertainties. For example, whether the metallic cores of relatively small differentiated impacting bodies would fail to re-equilibrate chemically in a terrestrial magma ocean, as required by the low-pressure models, depends on the extent to which the cores would emulsify — a question that is currently poorly understood (Rubie et al., 2007). On the other hand, a recent re-evaluation of the partitioning of Ni and Co has shown that if high-pressure metal–silicate equilibration occurred in a single stage scenario (i.e. constant pressure, temperature and oxygen fugacity), the partition coefficients would not converge with increasing pressure to a value that is consistent with the near chondritic Ni/Co ratio in the mantle (Kegler et al., 2008).

An improved understanding of core formation may be achieved by considering not only the refractory siderophile elements but also other classes of elements, such as refractory lithophile elements and volatile elements (Fig. 1). In particular, some refractory lithophile elements such as Nb and Ta, which show little or no depletion in the mantle, can become siderophile at very reducing conditions. As these elements are not depleted significantly from the mantle, any model which requires conditions that would lead to their depletion can be excluded. One of the aims of the present study is to investigate how the partitioning of these elements, together with Si and the weakly-siderophile element V, depends on pressure, temperature and oxygen fugacity. Using our results for Nb and V, we show that the conditions implied by low-pressure core-formation models (Wänke, 1981; O'Neill, 1991) are incompatible with the concentrations of some refractory lithophile elements in the mantle and that high-pressure metal–silicate equilibration must have occurred during core formation.

We also provide additional constraints on the conditions of core formation by studying the high-pressure, high-temperature partitioning of the volatile elements Mn, Ga, Zn and In. These elements plot on a trend of increasing depletion from the mantle as a function of their 50% condensation temperatures, which is referred to as the volatility trend (Fig. 1). This implies that their depletion in the Earth's mantle mainly results from early volatile loss from the inner solar system. The Ga/Mn and In/Zn ratios are near-chondritic and thus appear not to have been significantly fractionated during core-mantle differentiation or late accretion processes. However, we use experimentally derived constraints to demonstrate that Mn, Ga, In and Zn become siderophile under certain conditions. By considering the ratios of their partition coefficients, we show that metal–silicate equilibration at low pressures would have caused severe fractionation of the respective element pairs, thus supporting, again, the importance of very high pressure equilibration during core formation.

2. EXPERIMENTAL METHODS AND RUN PRODUCTS

Metal–silicate partitioning experiments were performed in multianvil and piston cylinder devices. Synthetic peridotite melts were equilibrated with Fe-rich metallic liquids at 2–24 GPa and 2023–2873 K at oxygen fugacities such that

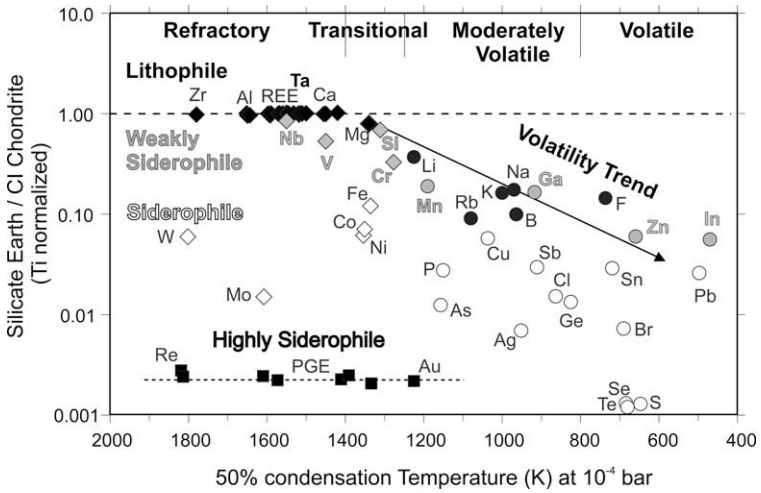

Fig. 1. Element abundances of the Earth's mantle normalised to CI chondrite and Ti (data from Palme and O'Neill, 2003). Siderophile elements have metal–silicate partition coefficients that are >1 and were therefore depleted from the mantle relative to CI during core formation. They can be divided into three basic groups, weakly siderophile (grey symbols), siderophile (unfilled symbols) and highly siderophile (black squares). Lithophile elements are not depleted from the mantle as a result of core formation (all other black symbols). An additional depletion trend affecting both lithophile and siderophile elements results from volatile behaviour (circles) which is considered to be a broad function of the elements' 50% condensation temperatures from the solar nebula at 10^{-4} bar (data from Wasson, 1985).

the equilibrated Fe-rich liquid alloy contained 0–19.6 mol% Si. The experiments were performed on three sets of starting materials each of which consisted of 55–56 wt% synthetic peridotite and 34–40 wt% Fe-rich metal, together with additional components that were added as oxides at concentration levels of 0.5–2 wt% (Table 1). Ti, Cr, Mn, and Ta were added to all starting mixtures, Ga, In and Zn were added to set "A", Nb and V to set "B", and all of these elements were added to set "C". The metallic component of the starting materials contained Fe, Si, Ni and Co, and in some cases S (Table 1).

The synthetic peridotite was prepared from major element oxides with a primitive mantle composition containing ~8 wt% FeO, as reported by Palme and O'Neill (2003). Mixtures of pure, dried powders of MgO, SiO_2, Al_2O_3, TiO_2, MnO, Cr_2O_3, $CaCO_3$ and Fe_2O_3 were decarbonated in air at 1273 K and afterwards reduced in a CO–CO_2 atmosphere at 1473 K and 2 log fo_2 units below the fayalite–magnetite–quartz buffer. The Fe-rich metal mixture always contained 2 wt% Ni and 1 wt% Co and variable proportions of Si (0.1–16.5 wt%) which was added in the form of either $Fe_{84}Si_{16}$ or $Fe_{71}Si_{29}$ alloy. The addition of metallic Si enabled the oxygen fugacity to be varied from −1.3 to −4.2 log units relative to the iron-wüstite buffer (ΔIW-1.3 to ΔIW-4.2). Three experiments were performed with 7.0, 9.9 and 24.5 wt% S in the metallic fraction of the starting composition (added as FeS), and all other experiments were S-free (Table 1).

In the high-pressure experiments, the samples were contained in either graphite or single-crystal MgO capsules; as discussed below, neither material is ideal. Both types of capsule react chemically with the sample, thus limiting run durations to between 20 s and 25 min depending on temperature (Table 2).

The experimental conditions are listed in Table 2. Three experiments were performed at 2 GPa and 2013–2023 K, in a piston-cylinder apparatus using a talc-pyrex pressure assembly and graphite furnace. In experiment P1 (Table 2) three graphite capsules, each containing a different starting material, were run together at 2013 K. In experiments C15 and CDF1, two and five MgO capsules, respectively, were run together, each with different starting materials (Table 2). All other experiments were carried out in multianvil presses employing Cr_2O_3-doped MgO octahedra as the pressure medium. For the experiments at 6 and 18 GPa, octahedra with 18 mm edge lengths and tungsten carbide cubes with 11 mm truncations (18/11 configuration) were used in a 500-tonne Walker-type multianvil and a 5000-tonne Kawai-type multianvil system, respectively. Experiments at 20 GPa were performed in 10/5 assemblies in a 1000-tonne Kawai-type press. A 1200-tonne Kawai-type press with a 10/4 assembly was used to reach 24 GPa. For 18/11 assemblies, the use of stepped $LaCrO_3$ heaters ensured that the temperature gradient across the sample was minimised (Rubie, 1999). At each pressure between 2 and 20 GPa the effect of fo_2 on the partitioning behaviour was studied at constant T. Additionally, we have varied the temperature in isobaric runs at 6 and 18 GPa.

For the piston-cylinder run P1 the temperature was measured using a type R Pt–$Pt_{87}Rh_{13}$ thermocouple. In all other experiments, type D $W_{97}Re_3$–$W_{75}Re_{25}$ thermocouples were employed. For experiments above 2273 K the thermocouple reading is usually less reliable and for isothermal experiments the same power value was used. On extrapolating to temperatures ⩾2573 K and in cases where thermocouples failed (Table 2), the temperature was estimated from the temperature versus power relationship derived from the most stable thermocouple readings. Based on variations in the temperature–power calibrations, the maximum temperature uncertainty is ±150 K above 2573 K; at lower temperatures the uncertainty is estimated to be ±100 K. The

Table 1
Compositions of the starting materials (wt%).

Series:	(A)					(B)			(C)	
	A-1	A-5	A-2	A-3	A-4	A-R5	A-R2	A-R-S1	A-RV1-S1	A-RV2-S2
SiO_2	25.65	25.65	25.65	25.65	25.65	25.37	25.37	25.37	25.32	25.32
MgO	20.77	20.77	20.77	20.77	20.77	20.55	20.55	20.55	20.51	20.51
Al_2O_3	2.54	2.54	2.54	2.54	2.54	2.51	2.51	2.51	2.50	2.50
CaO	2.06	2.06	2.06	2.06	2.06	2.04	2.04	2.04	2.04	2.04
FeO	4.58	4.58	4.58	4.58	4.58	4.53	4.53	4.53	4.52	4.52
TiO_2	0.12	0.12	0.12	0.12	0.12	2.00	2.00	2.00	0.12	0.12
Cr_2O_3	0.21	0.21	0.21	0.21	0.21	1.50	1.50	1.50	1.00	1.00
MnO	0.08	0.08	0.08	0.08	0.08	1.50	1.50	1.50	2.00	2.00
Ta_2O_5	2.00	2.00	2.00	2.00	2.00	1.50	1.50	1.50	2.00	2.00
Nb_2O_5	—	—	—	—	—	1.50	1.50	1.50	2.00	2.00
V_2O_5	—	—	—	—	—	2.00	2.00	2.00	1.00	1.00
Ga_2O_3	1.00	1.00	1.00	1.00	1.00	—	—	—	1.00	1.00
In_2O_3	0.50	0.50	0.50	0.50	0.50	—	—	—	1.00	1.00
ZnO	0.50	0.50	0.50	0.50	0.50	—	—	—	1.00	1.00
Fe	32.20	35.60	37.00	38.40	38.76	31.15	32.38	29.05	26.89	23.29
Si	6.60	3.20	1.80	0.40	0.04	2.80	1.58	2.45	2.72	1.36
S	—	—	—	—	—	—	—	2.45	3.37	8.33
Ni	0.80	0.80	0.80	0.80	0.80	0.70	0.70	0.70	0.68	0.68
Co	0.40	0.40	0.40	0.40	0.40	0.35	0.35	0.35	0.34	0.34

samples were quenched rapidly by switching off the electric power and were then slowly decompressed.

Typical run products contain a "sphere" of quenched metal that separated from the silicate while both phases were in the molten state. Fig. 2a shows a section through sample Z442 that was recovered from 18 GPa and 2573 K and was contained in a MgO single-crystal capsule. When using such capsules, the MgO reacts with the silicate melt resulting in patches of ferropericlase that sometimes form a discontinuous rim around the metal "spheres". When employing graphite capsules, C dissolves in the Fe-rich liquid and the quenched metal often contains laths of graphite. Moreover, melt sometimes infiltrated into the capsule wall especially in samples run at 20 GPa in which the graphite transformed to diamond.

Both metal and silicate phases developed heterogeneous textures during the quench. Fig. 2b shows a relatively coarse quench texture in the metal phase from sample V307 run at 6 GPa and 2373 K under very reducing conditions. Ta-rich flower-shaped quench crystals have exsolved in a heterogeneous matrix. Depending on the starting composition, such quench crystals can also contain either Ga and In or Nb and V. In samples starting from composition (B), in addition to these crystals the typical quench phenomenon consist of small rounded blobs up to 5 μm in diameter that are enriched in O, Si, Mn, Cr, V, Ti, Ta and Nb relative to the surrounding metal matrix and consist of silicates and oxides (Fig. 2c and d). Similar textures have been observed frequently and are interpreted as the products of quench-induced exsolution in a metallic liquid that was homogeneous at run conditions (e.g. Gessmann and Rubie, 1998; O'Neill et al., 1998; Chabot and Agee, 2003).

An example of a silicate quench texture is shown in Fig. 2e. Large elongated skeletal olivine crystals are the characteristic feature in samples that were equilibrated at pressures up to 6 GPa. The interstitial matrix is enriched in Fe, Ca and Al and contains exsolved phases that are enriched in trace elements. At pressures of 18–24 GPa the textures are usually less coarse which makes the analysis of the quenched silicate liquid much easier. Only in sample V307, run under the most reducing conditions at 6 GPa, did the silicate melt quench to a glass.

3. ANALYTICAL TECHNIQUES

Quantitative analysis of both metal and silicate phases were performed using a JEOL JXA-8200 electron probe micro-analyzer (EPMA). In all cases an accelerating voltage of 20 kV and a beam current of 50 nA were applied. Peak counting times were 20 s for Mg, Al, Ca, Fe and Si in the silicate phase and for Fe in the quenched metals. For the minor and trace elements (Ta, Nb, Ti, V, Cr, Mn and Ga, In, Zn) counting times of 120–180 s were used for both silicate and metal phases as well as for Si in the metal. Ni, Co and S were analyzed for 120–180 and 40–60 s in silicate and metal, respectively. A series of pure metals, silicates, oxides, arsenides (GaAs, InAs) and sulphides (ZnS, FeS_2) were employed as standards. Ta, Nb and In were analyzed using their L_α lines whereas for Ga the $K_{\beta 1}$ line had to be used as its other peaks overlap with those of Ta and In. All microprobe data were corrected using the phi–rho–*z* routine. The oxygen content of the silicate phase was calculated by stoichiometry. The results of the analyses are listed in Table 3.

When using graphite capsules, some carbon inevitably dissolved in the liquid metal at run conditions. As carbon was not measured by EPMA, the analyses of these quenched metals have totals of less than 100% (Table 3). We used the difference between the obtained totals and 100% as an estimate of the carbon concentration from which we calculated the mole fractions of carbon in these

Table 2
Details of the experimental conditions; Si, C and S contents of the quenched metal melt and Mg/Si ratio of the quenched silicate melt.

Run	Starting comp.	Capsule material	t (s)	P (GPa)	T (K)	log fo_2 (ΔIW)	Quenched metal melt			Quenched silicate melt
							X_C	X_S	X_{Si}	Mg/Si[b]
							(mole fractions)			
P1-19	A-5	Graphite	70	2	2013	−4.04	0.156	—	0.050	0.97
P1-21	A-2	Graphite	70	2	2013	−3.19	0.279	—	0.003	0.97
P1-20	A-3	Graphite	70	2	2013	−1.78	0.223	—	0.000	1.31
CDF1-5	A-5	MgO	120	2	2023	−3.18	—	—	0.078	1.03
C15-9	A-R5	MgO	150	2	2023	−3.02	—	—	0.041	1.23
CDF1-2	A-2	MgO	120	2	2023	−2.71	—	—	0.024	1.14
C15-10	A-R2	MgO	150	2	2023	−2.29	—	—	0.004	1.28
CDF1-3	A-3	MgO	120	2	2023	−1.51	—	—	0.000	1.08
CDF1-4	A-4	MgO	120	2	2023	−1.37	—	—	0.000	1.17
CDF1-1	A-RV2S2	MgO	120	2	2023	−1.39	—	0.390	0.001	1.23
V307	A-1	Graphite	300	6	2373[a]	−4.20	0.043	—	0.187	0.97
V312	A-5	Graphite	1500	6	2373	−3.24	0.149	—	0.036	1.23
V334	A-R5	Graphite	600	6	2373	−2.65	0.245	—	0.002	1.03
V310	A-2	Graphite	1500	6	2373[a]	−2.27	0.227	—	0.002	1.05
V337	A-R2	Graphite	600	6	2373[a]	−1.89	0.232	—	0.000	1.20
V309	A-3	Graphite	900	6	2373[a]	−1.40	0.249	—	0.000	1.16
V311	A-4	Graphite	1500	6	2373[a]	−1.37	0.225	—	0.000	1.30
V346	A-R5	MgO	300	6	2373	−3.57	—	—	0.027	1.88
V366	A-R5	MgO	130	6	2373	−3.41	—	—	0.029	2.02
V365	A-R2	MgO	120	6	2373	−2.84	—	—	0.004	2.09
V367	A-R5	MgO	120	6	2573[a]	−3.39	—	—	0.032	2.20
V397	A-RV1S1	MgO	60	9	2373	−3.49	—	0.173	0.019	1.39
Z457	A-3	MgO	90	18	2473	−1.59	—	—	0.002	1.27
Z442	A-5	MgO	90	18	2573	−2.78	—	—	0.082	1.39
Z469	A-R5	MgO	90	18	2573	−2.50	—	—	0.056	1.54
Z474	A-R2	MgO	95	18	2573	−2.04	—	—	0.030	1.45
Z448	A-5	MgO	20	18	2823[a]	−2.71	—	—	0.090	1.40
Z551	A-RS1	MgO	120	18	2573[a]	−2.47	—	0.125	0.020	1.49
H2333	A-1	Graphite	330	20	2373[a]	−3.39	0.216	—	0.057	1.08
H2340	A-5	Graphite	480	20	2373[a]	−2.25	0.313	—	0.000	1.13
H2347	A-3	Graphite	320	20	2373	−1.64	0.279	—	0.000	1.16
H2350	A-4	Graphite	285	20	2373	−1.31	0.255	—	0.000	1.17
S3658	A-5	MgO	90	24	2873[a]	−2.56	—	—	0.095	1.15

t, run duration; P, pressure; T, temperature.
fo_2, oxygen fugacity calculated relative to the IW buffer (see Appendix).
MgO, MgO single-crystal capsule.
[a] Derived from temperature vs. power relationship; all other temperatures from thermocouple readings.
[b] Mg/Si ratio: mol% basis.

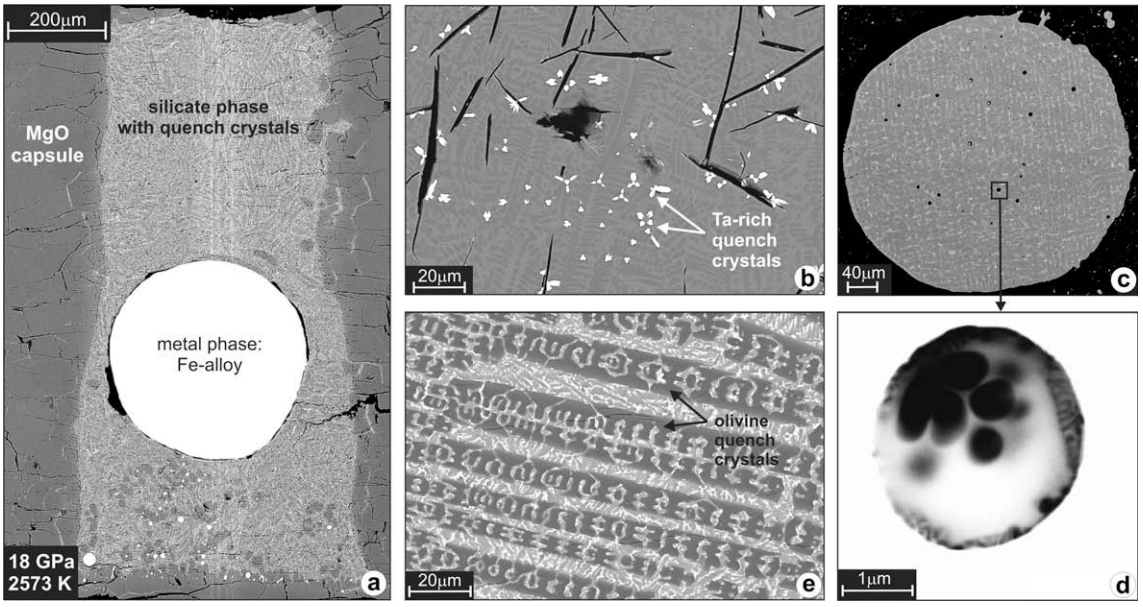

Fig. 2. Back scattered electron images showing characteristic features of the run products. (a) Full section through sample Z442 (18 GPa, 2573 K) contained in a MgO single-crystal capsule. The metal sphere had separated from the silicate liquid at run conditions. (b) Detail of the quench texture of the metal phase in sample V307 (6 GPa, 2373 K). Under very reducing conditions up to 3.4 wt% Ta can be found in the metal phase resulting in the formation of flower-shaped crystals upon quenching; the darker grey areas of the matrix are richer in Si, Ni and Co compared to the brighter grey ones; black features are cracks. (c and d) Quench texture in the large metal blob of sample V365 (6 GPa, 2373 K). Small rounded blobs (black in c) of an average diameter of 2–3 μm occur in the grey matrix of the blob that additionally shows a dendritic quench pattern. (d) Close-up of one of the quench blobs in (c), revealing a heterogeneous composition using a different contrast for the BSE image. (e) Typical silicate quench texture, sample V311 (6 GPa, 2373 K). The quenched silicate melt has formed elongated skeletal olivine crystals. The brighter grey matrix is enriched in Fe, Ca and Al and in this example, under more oxidised conditions, exsolved Ta-, Ga- and In-rich phases (white flakes).

metals (X_C) as listed in Table 2. These estimated carbon concentrations therefore depend on the accuracy of the totals and could represent a minimum if some of the graphite laths, which were avoided during analysis, formed during the quench.

In order to account for the heterogeneous quench textures (Fig. 2b and e) both silicate and metal phases were analyzed using a defocused electron beam (with diameters of 20–30 μm for silicate, 10–20 μm for metal). For samples in which the quenched metal contains irregularly distributed quench crystals several microns in size, the bulk metal composition was calculated from the volume fractions, the densities and the compositions of the phases present (quench crystals were analyzed with a focused electron beam) (compare O'Neill et al., 1998). The volumetric proportions within the large metal "spheres" were derived from the area proportions of matrix and quench crystals determined from image analysis of BSE images of the entire spheres assuming that the analyzed sections are representative for the whole sphere. Image analysis was performed using public domain software ImageJ 1.34s (National Institute of Health, USA). When areas larger than 20 μm × 20 μm are required to obtain a representative analysis, the applied image analysis produces results that are better from those obtained by rastering areas with the electron beam.

In some samples, depending on the capsule material, a carbon or MgO rim formed at the metal–silicate interface. To ensure that this did not inhibit equilibration between silicate and metal liquids we also analyzed smaller metal spheres that were in direct contact with the silicate and found compositions identical to those of the large spheres. In most samples we analyzed the metals along profiles across the spheres, which showed the absence of compositional zoning. Additionally, we found no systematic variation of the quenched silicate liquid composition over the respective capsule sections.

In samples equilibrated at the extreme ends of the studied redox range, some trace element concentrations are very low in one of the respective phases. Therefore, one should note that for some elements in some samples the EPMA results represent an upper limit. Such values are indicated in Table 3.

We also determined ferropericlase compositions in some samples contained in MgO single-crystal capsules (sample numbers and results see Table 4; peak counting times: Mg 20 s; Fe, Ca, Si, Ni and Co, 30–60 s; Al 120 s; all other trace elements 180 s). For these analyses we chose small patches of ferropericlase that were in direct contact with either the large metal sphere or small metal spheres. Additionally, we analyzed the wall of the MgO capsule close to the interface with the sample where a brighter grey tone in the BSE image due to a higher Fe content indicates a diffusive reaction rim.

4. RESULTS

Experimental run durations varied from 20 to 1500 s. Run durations in MgO capsules were generally limited to

Table 3
Average compositions of the quenched silicates and metals (wt%); table continues on the next two pages; footnotes for all at bottom of last table.

Silicate	**P1-19**		**P1-21**		**P1-20**		**CDF1-5**		**C15-9**		**CDF1-2**		**C15-10**		**CDF1-3**		**CDF1-4**		**CDF1-1**		**V307**	
	No = 29	±2σ[a]	No = 30	±2σ	No = 27	±2σ	No = 9	±2σ	No = 9	±2σ	No = 9	±2σ	No = 26	±2σ	No = 10	±2σ	No = 9	±2σ	No = 9	±2σ	No = 78	±2σ
Si	25.26	0.39	24.29	0.55	20.49	0.50	23.63	2.86	20.21	0.70	22.90	1.93	18.75	0.55	20.65	1.07	19.56	1.06	18.82	0.41	25.72	0.92
Mg	21.31	0.99	20.43	1.57	23.24	1.13	21.12	9.61	21.58	3.51	22.57	7.10	20.79	5.04	19.39	8.25	20.08	12.51	20.34	12.53	21.51	0.95
Al	2.76	0.28	2.84	0.29	2.17	0.62	2.92	1.71	2.18	0.59	2.58	1.24	2.17	0.79	3.31	1.86	3.01	2.78	2.71	2.45	2.50	0.43
Ca	3.23	0.25	3.14	0.29	2.27	0.34	3.49	2.47	2.58	0.79	2.95	1.66	2.57	1.08	3.63	2.25	3.36	3.51	3.44	3.23	2.91	0.71
Fe	0.29	0.12	0.82	0.28	5.60	0.82	0.78	0.15	1.01	0.02	1.58	0.13	2.56	0.18	6.80	0.86	8.57	2.28	4.27	1.19	0.23	0.23
Co	l.o.d.	-	l.o.d.	-	0.01[d]	0.01	l.o.d.	-	l.o.d.	-	l.o.d.	-	l.o.d.	-	<0.01[d]	0.01	0.01	0.01	0.01	0.01	0.01[d]	0.01
Ni	l.o.d.	-	l.o.d.	-	<0.01[d]	0.01	l.o.d.	-	l.o.d.	-	l.o.d.	-	l.o.d.	-	l.o.d.	-	l.o.d.	-	l.o.d.	-	l.o.d.	-
Ti	0.11	0.02	0.13	0.02	0.10	0.07	0.11	0.07	1.78	0.45	0.09	0.05	1.85	0.72	0.14	0.09	0.18	0.19	0.14	0.13	0.11	0.03
V	-	-	-	-	-	-	-	-	0.80	0.05	-	-	1.23	0.10	-	-	-	-	0.55	0.27	-	-
Cr	0.02	0.01	0.05	0.02	0.13	0.03	0.10	0.03	0.60	0.05	0.12	0.04	0.97	0.18	0.19	0.06	0.19	0.08	0.47	0.25	0.01[d]	0.02
Mn	0.14	0.02	0.13	0.02	0.11	0.03	0.16	0.06	1.83	0.16	0.20	0.04	1.84	0.33	0.14	0.04	0.09	0.04	2.44	1.10	0.11	0.03
Ta	0.38	0.11	2.88	0.57	2.43	0.35	2.98	1.73	1.93	0.58	2.93	1.58	2.07	0.77	3.53	2.32	3.03	2.88	3.17	3.05	0.10	0.17
Nb	-	-	-	-	-	-	-	-	0.68	0.21	-	-	1.49	0.59	-	-	-	-	2.46	2.47	-	-
Ga	0.03[e]	0.07	0.06[e]	0.09	0.29	0.10	<0.01[d]	0.04	-	-	0.02[d]	0.07	-	-	0.08	0.09	0.12	0.17	0.46	0.39	0.04[e]	0.03
In	0.07[e]	0.02	0.09	0.02	0.15	0.03	0.06[d]	0.02	-	-	<0.06[d]	0.02	-	-	0.09	0.04	0.10	0.06	0.084	0.05	0.07[e]	0.06
Zn	0.13	0.01	0.22	0.01	0.45	0.09	0.13	0.04	-	-	0.18	0.03	-	-	0.45	0.11	0.46	0.14	0.79	0.37	<0.12	0.05
W	l.o.d.	-	l.o.d.	-	<0.01[d]	0.01	-	-	-	-	-	-	-	-	-	-	-	-	-	-	-	-
S	-	-	-	-	-	-	-	-	-	-	-	-	-	-	-	-	-	-	0.32	0.30	-	-
O calc.[b]	46.87		45.97		43.93		45.86	0.54	43.08		45.73	0.42	41.93		43.73	0.95	42.97	1.86	43.09	2.41	47.08	
Total	100.61		101.07		101.36		101.34	1.30	98.26		101.93	0.99	98.22		102.15	1.03	101.74	2.00	103.57	1.27	100.52	
Metal	**P1-19**		**P1-21**		**P1-20**		**CDF1-5**		**C15-9**		**CDF1-2**		**C15-10**		**CDF1-3**		**CDF1-4**		**CDF1-1**		**V307**	
	No = 30	±2σ[a]	No = 32	±2σ	No = 30	±2σ	No = 4	±2σ	No = 35	±2σ	No = 8	±2σ	No = 34	±2σ	No = 8	±2σ	No = 7	±2σ	No = 14	±2σ	No = 17	±2σ
Si	2.90	0.21	0.19	0.10	$<10^{-3}$[d]	0.00	4.04	0.01	2.07	0.11	1.23	0.04	0.23	0.08	l.o.d.	-	l.o.d.	-	0.03[e]	0.18	10.45	1.30
Fe	83.87	1.45	85.43	3.32	88.17	1.19	89.27	0.48	89.48	0.94	91.86	2.35	94.98	0.74	93.24	1.76	93.49	1.96	65.06	4.79	79.29	6.76
Co	0.91	0.04	0.85	0.10	1.07	0.07	0.94	0.01	0.93	0.16	0.99	0.03	1.08	0.08	1.08	0.13	1.06	0.09	1.00	0.36	0.84	0.15
Ni	1.79	0.09	1.53	0.24	1.98	0.19	1.84	0.03	1.75	0.34	1.89	0.05	1.81	0.06	1.95	0.50	1.83	0.24	1.63	0.72	1.53	0.31
Ti	0.01[d]	0.01	<0.01[d]	0.01	$2*10^{-3}$[d]	0.01	$<2*10^{-3}$[d]	$3*10^{-3}$	$<4*10^{-3}$[d]	0.01	$<10^{-3}$[d]	10^{-3}	$<3*10^{-3}$	$<4*10^{-3}$[d]	l.o.d[d]	-	$<10^{-3}$[d]	$<4*10^{-3}$[d]	$<10^{-3}$[d]	$<2*10^{-3}$[d]	0.04[e]	0.1
V	-	-	-	-	-	-	-	-	1.35	0.01	-	-	0.56	0.03	-	-	-	-	0.36	0.23	-	-
Cr	0.36	0.03	0.40	0.06	0.10	0.06	0.30	0.01	1.44	0.02	0.19	0.01	0.95	0.03	0.04	0.01	0.03	0.01	0.84	0.47	0.33	0.09
Mn	0.07	0.03	<0.01[d]	0.02	$<10^{-3}$[d]	$4*10^{-3}$	<0.01[d]	0.01	0.19	0.05	<0.01[d]	0.01	0.05	0.01	l.o.d.	-	l.o.d.	-	0.34	0.13	<0.04[e]	0.1
Ta	2.02	1.54	1.37	0.49	<0.01[d]	0.03	0.42	0.03	0.14	0.07	0.10	0.04	0.01[d]	0.02	<0.01[d]	0.02	<0.04[e]	0.17	<0.02[d]	0.08	3.43[e]	7.92
Nb	-	-	-	-	-	-	-	-	1.53	0.34	-	-	0.38	0.07	-	-	-	-	<0.02	0.04	-	-
Ga	2.54	0.28	1.56	0.89	2.05[e]	1.17	2.20	0.12	-	-	2.34	0.18	-	-	2.46	0.18	2.51	0.26	1.92	1.27	1.60	0.13
In	0.85	0.18	0.71	0.16	0.73	0.27	0.85	0.06	-	-	0.89	0.03	-	-	0.94	0.05	1.03	0.08	1.38	1.48	0.79	1.11
Zn	0.82	0.06	0.36	0.19	0.10	0.05	0.84	0.01	-	-	0.70	0.01	-	-	0.34	0.08	0.24	0.05	0.46	1.28	0.58	0.20
W	0.02[d]	0.023	l.o.d.	-	0.01[d]	0.02	-	-	-	-	-	-	-	-	-	-	-	-			-	-
S	-	-	-	-	-	-	-	-	-	-	-	-	-	-	-	-	-	-	26.38	5.68	-	-
Total	96.16[c]		92.43[c]		94.22[c]		100.73		98.89		100.21		100.05		100.07		100.24		99.44		98.92[d]	
silicate	**V312**		**V334**		**V310**		**V337**		**V309**		**V311**		**V346**		**V366**		**V365**		**V367**		**V397**	
	No = 19	±2σ[a]	No = 40	±2σ	No = 43	±2σ	No = 37	±2σ	No = 24	±2σ	No = 60	±2σ	No = 31	±2σ	No = 26	±2σ	No = 24	±2σ	No = 26	±2σ	No = 12	±2σ
Si	21.14	2.38	22.36	0.89	22.80	0.45	19.92	0.30	19.37	0.57	18.40	0.42	16.98	8.21	16.62	0.80	16.12	0.56	15.93	0.72	19.97	2.76
Mg	22.43	1.65	20.01	1.18	20.72	0.99	20.76	2.07	19.52	7.05	20.67	4.41	27.66	23.31	29.07	2.42	29.20	1.39	30.26	1.27	24.06	7.00
Al	5.13	4.00	2.23	0.23	2.37	0.20	1.97	0.39	2.65	1.57	2.30	1.01	1.80	7.39	1.52	0.70	1.20	0.18	1.23	0.32	2.44	1.45
Ca	2.88	0.61	3.00	0.28	2.77	0.28	2.25	0.46	2.82	1.67	2.59	1.19	2.96	10.76	2.42	1.30	1.75	0.58	1.79	0.70	2.76	1.72
Fe	0.88	0.56	1.56	0.31	2.77	0.31	4.55	0.24	9.06	1.07	10.05	1.42	0.74	1.04	0.94	0.26	1.96	0.32	1.05	0.26	1.30	0.41
Co	<0.01[d]	0.01	l.o.d.	-	0.01[d]	0.02	0.01[d]	0.01	0.02[d]	0.02	0.03[d]	0.03	l.o.d.	-	l.o.d.	-	l.o.d.	-	l.o.d.	-	l.o.d.	-

Ni	0.01[d]	0.02	l.o.d.	-	l.o.d.	-	l.o.d.	-	0.01[d]	0.02	l.o.d.	-	l.o.d.	-	l.o.d.	-	l.o.d.	-	l.o.d.	-	l.o.d.	-
Ti	0.08	0.02	1.86	0.32	0.13	0.02	1.78	0.36	0.15	0.09	0.11	0.05	1.81	6.36	1.48	0.65	1.32	0.38	1.21	0.32	0.11	0.07
V	-	-	0.51	0.04	-	-	1.00	0.09	-	-	-	-	0.59	1.31	0.57	0.14	0.65	0.05	0.52	0.06	0.42	0.15
Cr	0.10	0.13	0.38	0.03	0.071	0.027	0.68	0.06	0.13	0.05	0.14	0.06	0.32	0.80	0.32	0.09	0.44	0.04	0.30	0.05	0.28	0.11
Mn	0.08	0.01	1.65	0.11	0.14	0.03	1.64	0.11	0.11	0.03	0.13	0.04	1.01	1.76	1.10	0.28	1.11	0.18	0.91	0.14	1.64	0.49
Ta	0.67	0.10	1.60	0.58	2.60	0.52	1.76	0.56	2.84	1.69	2.66	1.45	2.11	8.54	1.58	0.78	1.41	0.48	1.39	0.61	2.49	1.58
Nb	-	-	0.35	0.11	-	-	1.18	0.34	-	-	-	-	0.97	3.88	0.80	0.40	1.04	0.36	0.75	0.32	1.11	0.78
Ga	0.11	0.04	-	-	0.23	0.03	-	-	0.80	0.44	0.73	0.29	-	-	-	-	-	-	-	-	0.06[d]	0.09
In	0.10	0.06	-	-	0.14	0.03	-	-	0.34	0.18	0.30	0.11	-	-	-	-	-	-	-	-	0.06[d]	0.02
Zn	0.22	0.05	-	-	0.42	0.02	-	-	0.53	0.05	0.50	0.04	-	-	-	-	-	-	-	-	0.39	0.08
W	l.o.d.	-	l.o.d.	-	<0.01[d]	0.02	l.o.d.	-	l.o.d.	-	l.o.d.	-	l.o.d.	-	-	-	-	-	-	-	-	-
S	-	-	-	-	-	-	-	-	-	-	-	-	-	-	-	-	-	-	-	-	0.18	0.17
O calc.[b]	45.15		44.55		44.50		43.28		42.12		41.58		42.84		42.65		41.91		41.88		44.20	0.83
Total	98.98		100.06		99.68		100.81		100.48		100.19		99.80		99.08		98.10		97.21		101.47	2.24

metal	**V312**		**V334**		**V310**		**V337**		**V309**		**V311**		**V346**		**V366**		**V365**		**V367**		**V397**	
	No = 37	±2σ[a]	No = 42	±2σ	No = 38	±2σ	No = 35	±2σ	No = 46	±2σ[a]	No = 40	±2σ	No = 37	±2σ	No = 39	±2σ	No = 33	±2σ	No = 32	±2σ	No = 8	±2σ
Si	2.06	0.20	<0.13[e]	0.35	<0.12[e]	0.14	l.o.d.	-	0.02[d]	0.08	<0.02[d]	0.06	1.36	0.10	1.44	0.07	0.22	0.11	1.64	0.10	1.00	0.92
Fe	86.40	1.58	80.68	2.81	87.21	1.49	87.15	1.15	88.31	3.53	89.86	1.78	90.15	2.54	90.03	1.43	94.18	1.05	90.43	1.95	72.31	3.06
Co	1.03	0.07	1.05	0.32	0.93	0.07	1.04	0.17	1.05	0.11	0.93	0.15	0.97	0.05	0.93	0.02	1.09	0.08	0.93	0.02	1.05	0.06
Ni	1.77	0.16	1.77	1.45	1.72	0.22	1.85	0.79	1.78	0.36	1.87	0.73	2.03	0.26	1.75	0.07	1.93	0.23	1.72	0.08	2.05	0.27
Ti	0.01[d]	0.01	0.05	0.03	0.01[d]	0.01	0.01[e]	0.01	$3*10^{-3}$[d]	0.01	$<3*10^{-3}$[d]	0.01	<0.02[e]	0.01	<0.01[d]	0.01	$<3*10^{-3}$[d]	0.01	<0.01[d]	0.01	$4*10^{-3}$[d]	0.01
V	-	-	2.77	1.03	-	-	1.29	0.27	-	-	-	-	1.18	0.19	1.15	0.08	0.55	0.16	1.06	0.21	0.87	0.17
Cr	0.61	0.09	2.64	1.01	0.29	0.05	1.71	0.40	0.22	1.06	0.09	0.03	1.72	0.15	1.63	0.07	1.14	0.13	1.57	0.13	1.34	0.18
Mn	0.01[d]	0.07	0.42	0.10	0.02[e]	0.04	0.20	0.05	0.01	0.06	$2*10^{-3}$[d]	0.01	0.63	0.07	0.66	0.03	0.28	0.04	0.68	0.06	1.51	1.54
Ta	1.16	0.84	0.54	0.22	0.35	0.14	0.01[d]	0.02	<0.02[d]	0.04	0.02[d]	0.04	0.10[e]	0.13	0.12	0.08	0.01[d]	0.02	0.13[e]	0.15	0.23	0.12
Nb	-	-	3.46	2.22	-	-	0.57	0.55	-	-	-	-	0.99	1.39	1.16	0.71	0.26	0.47	1.14	1.21	2.36	0.51
Ga	1.83	0.58	-	-	2.19	0.62	-	-	1.18[e]	1.19	0.77[e]	0.81	-	-	-	-	-	-	-	-	2.68	0.19
In	0.92	0.21	-	-	0.88	0.29	-	-	0.60[e]	0.34	0.48[e]	0.44	-	-	-	-	-	-	-	-	2.17	0.89
Zn	0.52	0.09	-	-	0.26	0.08	-	-	0.12[e]	0.31	0.05[e]	0.03	-	-	-	-	-	-	-	-	1.59	0.62
W	l.o.d.	-	l.o.d.	-	<0.03[d]	0.04	<0.08	0.05	<0.03[d]	0.05	<0.02[d]	0.03	l.o.d.	-	-	-	-	-	-	-	-	-
S	-	-	-	-	-	-	-	-	-	-	-	-	-	-	-	-	-	-	-	-	10.45	1.08
Total	96.33[c]		93.51[c]		94.01[c]		93.92[c]		93.34[c]		94.12[c]		99.15		98.88		99.66		99.32		99.60	

silicate	**Z457**		**Z442**		**Z469**		**Z474**		**Z448**		**Z551**		**H2333**		**H2340**		**H2347**		**H2350**		**S3658**	
	No = 31	±2σ[a]	No = 34	±2σ	No = 33	±2σ	No = 34	±2σ[a]	No = 28	±2σ	No = 61	±2σ	No = 58	±2σ	No = 47	±2σ	No = 48	±2σ	No = 50	±2σ	No = 32	±2σ
Si	20.27	0.97	20.76	1.56	18.78	3.69	19.08	3.18	20.76	1.22	18.95	0.52	24.12	1.45	22.48	2.77	20.98	0.99	19.28	1.02	22.76	1.92
Mg	22.32	2.28	24.96	3.95	25.05	7.71	23.97	5.52	25.14	2.03	24.49	2.20	22.47	1.93	22.05	1.90	21.03	0.97	19.49	0.96	22.60	2.61
Al	1.91	0.36	2.02	0.21	1.85	0.33	1.63	0.16	1.80	0.30	1.63	0.14	2.37	1.37	2.05	1.51	2.53	0.29	1.87	0.23	1.94	0.37
Ca	2.65	0.82	2.58	1.38	1.70	2.45	1.80	2.07	2.70	0.44	2.07	0.74	3.17	1.13	3.04	1.01	2.64	0.17	2.87	0.08	3.04	0.49
Fe	7.25	0.66	1.60	0.32	2.34	0.81	3.38	1.12	1.85	0.39	2.08	0.30	0.64	0.46	2.78	1.41	6.24	0.73	9.79	0.95	1.91	0.74
Co	0.02	0.02	l.o.d.	-	0.01[d]	0.01	0.01[d]	0.01	l.o.d.	-	l.o.d.	-	l.o.d.	-	0.01[d]	0.01	0.02	0.01	0.03	0.01	<0.01[d]	0.01
Ni	0.01[d]	0.02	l.o.d.	-	l.o.d.	-	<0.01[d]	0.01	l.o.d.	-	l.o.d.	-	<0.01[d]	0.01	0.01[d]	0.01	<0.02	0.01	<0.02	0.01	<0.01[d]	0.02
Ti	0.07	0.02	0.13	0.06	1.54	2.38	1.32	1.03	0.10	0.02	1.49	0.42	0.14	0.03	0.06	0.01	0.06	0.01	0.14	0.01	0.12	0.02
V	-	-	-	-	0.96	0.41	0.94	0.28	-	-	0.88	0.07	-	-	-	-	-	-	-	-	-	-
Cr	0.13	0.02	0.07	0.02	0.57	0.19	0.64	0.16	0.07	0.02	0.52	0.04	0.03	0.01	0.28	0.07	0.17	0.03	0.15	0.02	0.13	0.10
Mn	0.05	0.02	0.09	0.03	1.04	0.56	1.16	0.37	0.08	0.03	1.15	0.19	0.07	0.03	0.08	0.03	0.11	0.02	0.05	0.02	0.09	0.02
Ta	1.87	0.79	1.96	1.64	1.36	3.15	1.14	1.40	1.94	0.64	1.58	0.85	0.62	0.75	1.68	1.52	2.82	0.66	3.22	0.69	2.60	1.32
Nb	-	-	-	-	0.93	1.98	0.88	1.05	-	-	0.88	0.45	-	-	-	-	-	-	-	-	-	-
Ga	0.26	0.09	0.05[e]	0.08	-	-	-	-	0.07[e]	0.07	-	-	0.17	0.11	0.62	0.09	1.23	0.13	1.48	0.12	0.12	0.11
In	0.12	0.03	0.05[e]	0.02	-	-	-	-	0.06[e]	0.014	-	-	<0.10[e]	0.06	0.27	0.04	0.46	0.03	0.64	0.01	0.09[e]	0.01
Zn	0.34	0.04	0.19	0.02	-	-	-	-	0.13	0.02	-	-	0.27	0.16	0.41	0.26	0.52	0.08	0.59	0.06	0.17	0.05
W	<0.01[d]	0.02	<0.01[d]	0.02	l.o.d.	-	l.o.d.	-	0.07	0.08	-	-	l.o.d.	-	<0.01[d]	0.01	l.o.d.	-	l.o.d.	-	0.01[d]	0.02

(*continued on next page*)

Table 3 (*continued*)

silicate	**Z457**		**Z442**		**Z469**		**Z474**		**Z448**		**Z551**		**H2333**		**H2340**		**H2347**		**H2350**		**S3658**	
	No = 31	±2σ[a]	No = 34	±2σ	No = 33	±2σ	No = 34	±2σ[a]	No = 28	±2σ	No = 61	±2σ	No = 58	±2σ	No = 47	±2σ	No = 48	±2σ	No = 50	±2σ	No = 32	±2σ
S	-	-	-	-	-	-	-	-	-	-	0.03	0.04	-	-	-	-	-	-	-	-	-	-
O calc.[b]	43.29		43.98		43.12		42.78		44.00		42.86		46.19		44.81		44.10		41.90		45.07	
Total	100.59		98.45		99.25		98.75		98.77		98.61		100.36		100.64		102.92		101.54		100.66	
metal	**Z457**		**Z442**		**Z469**		**Z474**		**Z448**		**Z551**		**H2333**		**H2340**		**H2347**		**H2350**		**S3658**	
	No = 45	±2σ[a]	No = 18	±2σ	No = 35	±2σ	No = 37	±2σ[a]	No = 34	±2σ	No = 37	±2σ	No = 33	±2σ	No = 43	±2σ	No = 36	±2σ	No = 32	±2σ	No = 34	±2σ
Si	0.12[d]	0.12	4.23	1.02	2.87	0.39	1.49	0.21	4.63	0.30	1.08	0.21	3.46	0.76	0.03[e]	0.14	10^{-3}[d]	0.01	$<10^{-3}$[d]	0.01	4.93	1.71
Fe	93.61	0.98	88.09	1.09	90.36	2.17	89.56	1.55	87.80	0.65	83.36	0.93	80.13	4.30	84.19	3.24	88.21	1.08	89.46	1.01	86.81	4.29
Co	1.11	0.07	0.87	0.31	1.04	0.05	1.04	0.11	0.96	0.11	1.00	0.02	0.98	0.09	1.05	0.26	1.01	0.35	0.96	0.31	1.14	0.79
Ni	2.11	0.13	1.32	0.65	1.99	0.16	2.01	0.20	1.76	0.29	1.90	0.08	1.81	0.29	1.92	1.50	2.02	1.83	1.97	1.51	2.13	1.18
Ti	10^{-3}[d]	0.01	<0.01	0.01	0.02[e]	0.01	0.01[e]	$4*10^{-3}$	$<2*10^{-3}$[d]	0.01	$4*10^{-3}$[d]	$3*10^{-3}$	0.03	0.01	$2*10^{-3}$[d]	0.01	10^{-3}[d]	0.01	$<10^{-3}$[d]	$4*10^{-3}$	$<2*10^{-3}$[d]	$4*10^{-3}$
V	-	-	-	-	0.56	0.30	0.35	0.16	-	-	0.86	0.04	-	-	-	-	-	-	-	-	-	-
Cr	0.06	0.03	0.26	0.05	1.35	0.19	1.00	0.18	0.26	0.02	1.59	0.08	0.85	0.16	1.75	0.56	0.21	0.13	0.08	0.06	0.31	0.16
Mn	10^{-3}[d]	0.01	0.06	0.02	0.59	0.07	0.39	0.05	0.07	0.02	0.70	0.10	0.27	0.04	0.06	0.02	0.02	0.02	$2*10^{-3}$[d]	0.01	0.08	0.04
Ta	<0.01[d]	0.03	0.75[e]	0.75	0.072[e]	0.15	<0.02[d]	0.04	0.25[e]	0.20	0.14	0.06	3.10	0.61	0.13	0.09	<0.01[d]	0.02	<0.01[d]	0.01	0.30[e]	0.46
Nb	-	-	-	-	0.64	1.47	0.32	0.72	-	-	1.25	0.14	-	-	-	-	-	-	-	-	-	-
Ga	2.18	0.19	2.49	0.17	-	-	-	-	2.39	0.14	-	-	2.22	0.43	0.96[e]	2.41	0.49[e]	1.05	0.37[e]	0.67	2.67	0.89
In	0.87[e]	0.69	0.92	0.20	-	-	-	-	0.86	0.14	-	-	0.86	0.30	0.46[e]	0.85	0.30[e]	0.60	0.27[e]	0.41	1.06	0.35
Zn	0.25	0.04	0.45	0.07	-	-	-	-	0.40	0.01	-	-	0.35	0.07	0.11[e]	0.20	0.04[e]	0.08	0.03[d]	0.08	0.32	0.09
W	0.02[d]	0.03	0.02[e]	0.03	l.o.d.	-	l.o.d.	-	0.64	0.30	-	-	0.28	0.16	0.45	0.18	<0.02[d]	0.03	0.02[d]	0.03	<0.01[d]	0.03
S	-	-	-	-	-	-	-	-	-	-	7.61	0.97	-	-	-	-	-	-	-	-	-	-
Total	100.34		99.47		99.48		96.19		100.03		99.50		94.35[c]		91.12[c]		92.34[c]		93.17[c]		99.77	

No. = number of analyses.

[a] Errors are given as two standard deviations of the respective population.

[b] Oxygen in silicate calculated by stoichiometry.

[c] Totals of metals from samples run in graphite capsules are <100 due to the likely presence of C which was not analyzed.

[d] Conc. close to or below the detection limit. l.o.d. limit of detection.

[e] Conc. less certain or overestimated with EPMA.

Table 4
Average compositions of ferropericlase from experiments contained in MgO single-crystal capsules (wt%).

wt%	C15-9		C15-10		V346		V366		V365		V367		Z457		Z442		Z448		Z551		S3658	
	No. = 6		No. = 5		No. = 4		No. = 8		No. = 8		No. = 9		No. = 7		No. = 9		No. = 9		No. = 8		No. = 7	
		±2σ[a]		±2σ		±2σ		±2σ		±2σ		±2σ		±2σ		±2σ		±2σ		±2σ		±2σ
SiO_2	0.13	0.41	0.07	0.13	0.13	0.27	<0.01[b]	0.02	0.04	0.07	0.38	1.61	0.12	0.03	0.12	0.02	0.09	0.02	0.13	0.11	0.09	0.02
MgO	93.71	5.15	89.07	6.13	93.62	3.99	95.53	3.57	92.53	4.69	94.05	5.00	83.55	1.86	94.83	0.90	95.55	0.63	91.76	3.52	95.74	1.36
Al_2O_3	1.01	0.34	1.26	0.62	1.70	0.56	0.97	0.37	0.91	0.32	1.03	0.69	1.29	0.05	1.53	0.05	1.28	0.14	1.19	0.41	1.23	0.07
CaO	<0.01[b]	0.01	<0.01[b]	0.01	0.03	0.01	0.02	0.01	0.03	0.03	0.07	0.23	0.04	0.03	0.04	0.01	0.05	0.02	0.02[b]	0.01	0.04	0.02
FeO	1.27	0.27	4.12	1.41	1.57	0.37	1.41	0.28	3.46	1.08	2.10	0.79	15.99	0.72	3.29	0.47	3.71	0.71	3.75	1.43	4.84	1.28
CoO	<0.01[b]	0.01	0.02	0.01	l.o.d.	—	0.01	0.01	0.01[b]	0.02	0.01[b]	0.01	0.07	0.01	0.01[b]	0.01	0.01[b]	0.02	0.02[b]	0.01	0.02[b]	0.03
NiO	<0.01[b]	0.02	0.02[b]	0.02	l.o.d.	—	l.o.d.	—	l.o.d.	—	l.o.d.	—	0.06	0.03	0.01[b]	0.02	0.02[b]	0.02	0.02[b]	0.02	0.02	0.03
TiO_2	1.52	1.01	1.54	0.98	0.97	0.44	0.61	0.49	0.58	0.39	0.68	0.56	0.02[b]	0.01	0.05	0.01	0.04	0.01	0.48	0.20	0.03	0.01
V_2O_3	1.81	2.39	2.53	1.96	1.66	1.21	1.14	1.44	1.91	1.96	1.27	1.31	—	—	—	—	—	—	1.58	1.37	—	—
Cr_2O_3	1.03	0.61	2.15	1.28	0.81	0.25	0.55	0.39	1.12	0.68	0.61	0.36	0.29	0.03	0.16	0.02	0.13	0.02	0.94	0.51	0.23	0.22
MnO	0.87	0.25	0.87	0.12	1.07	0.22	0.78	0.32	0.88	0.30	0.79	0.30	0.05	0.02	0.09	0.02	0.07	0.02	1.04	0.32	0.10	0.02
Ta_2O_5	0.14	0.15	0.11	0.11	0.05[b]	0.01	0.03[b]	0.04	0.04[b]	0.04	0.05[b]	0.15	0.04[b]	0.07	0.07	0.05	0.04[b]	0.07	0.03[b]	0.02	0.02[b]	0.07
Nb_2O_5	0.09	0.14	0.11	0.08	0.01[b]	0.03	0.01[b]	0.02	0.01[b]	0.02	0.03[b]	0.12	—	—	—	—	—	—	0.01[b]	0.01	—	—
Ga_2O_3	—	—	—	—	—	—	—	—	—	—	—	—	0.21	0.15	0.03[b]	0.07	0.07	0.11	—	—	0.07	0.11
In_2O_3	—	—	—	—	—	—	—	—	—	—	—	—	0.04[b]	0.01	0.03[b]	0.01	0.03[b]	0.01	—	—	0.04[b]	0.01
ZnO	—	—	—	—	—	—	—	—	—	—	—	—	0.83	0.03	0.46	0.02	0.28	0.02	—	—	0.45	0.06
Total	101.62	0.92	101.87	0.42	101.64	0.68	101.07	0.49	101.52	0.52	101.05	0.98	102.60	1.23	100.70	0.52	101.37	0.64	100.96	1.05	102.93	0.78

No. = number of analyses.
[a] Uncertainties are given as two standard errors of the respective population.
[b] Concentration close to the detection limit; l.o.d. limit of detection.

$\leqslant$300 s by the strong reaction between the silicate melt and the capsule, which ultimately leads to either escape or complete crystallisation of the melt. The very high temperatures should enable rapid equilibration between silicate and metal liquids (Thibault and Walter, 1995; Li and Agee, 2001). Corgne et al. (2008), for example, showed no difference in the metal–silicate partition coefficients for a range of similar elements to those studied here between experiments performed for 20 and 100 s, indicating that equilibrium may be reached in <20 s at 2273 K and 3.6 GPa. In our study, two experiments performed on an identical starting composition at 6 GPa and 2373 K for 130 and 300 s, respectively, showed no significant shift in partition coefficients for any element. In addition, in this time series the composition of ferropericlase at the wall of the capsule showed no significant change. We therefore conclude that within the time scale of our experiments equilibrium was achieved between both silicate and metal melts and the ferropericlase that formed on the inside wall of the original MgO capsule.

4.1. The exchange coefficient and effects of pressure and temperature on partitioning

The methods for the determination of oxygen fugacity in our partitioning experiments and the valence state of metal cations in the silicate phase are described in the Appendix together with details of how partition coefficients measured in graphite/diamond capsules were corrected for the presence of carbon dissolved in the liquid Fe phase.

The partitioning of an element M, with valence n, between metal and silicate can be expressed as an exchange reaction involving Fe and FeO:

$$\mathrm{MO}_{n/2}^{silicate} + \frac{n}{2}\mathrm{Fe}^{metal} = \mathrm{M}^{metal} + \frac{n}{2}\mathrm{FeO}^{silicate} \quad (1)$$

for which the equilibrium constant K can be written as

$$\log K_{(1)} = \frac{\left[a_M^{metal}\right]\left[a_{FeO}^{silicate}\right]^{\frac{n}{2}}}{\left[a_{MO_{n/2}}^{silicate}\right]\left[a_{Fe}^{metal}\right]^{\frac{n}{2}}} = \log\frac{\left[X_M^{metal}\right]\left[X_{FeO}^{silicate}\right]^{\frac{n}{2}}}{\left[X_{MO_{n/2}}^{silicate}\right]\left[X_{Fe}^{metal}\right]^{\frac{n}{2}}} + \log\frac{\left[\gamma_M^{metal}\right]\left[\gamma_{FeO}^{silicate}\right]^{\frac{n}{2}}}{\left[\gamma_{MO_{n/2}}^{silicate}\right]\left[\gamma_{Fe}^{metal}\right]^{\frac{n}{2}}} \quad (2)$$

with a, X and γ being the components' activities, mole fractions and activity coefficients, respectively. If we define an exchange coefficient K_D for any element M:

$$K_D^M = \frac{\left[X_M^{metal}\right]\left[X_{FeO}^{silicate}\right]^{\frac{n}{2}}}{\left[X_{MO_{n/2}}^{silicate}\right]\left[X_{Fe}^{metal}\right]^{\frac{n}{2}}} \quad (3)$$

then Eq. (2) can be rearranged to give:

$$\log K_D^M(P,T) = -\log K_{(1)} - \log\left[\frac{\gamma_M^{metal}}{\left(\gamma_{Fe}^{metal}\right)^{\frac{n}{2}}}\right] - \log\left[\frac{\left(\gamma_{FeO}^{silicate}\right)^{\frac{n}{2}}}{\gamma_{MO_{n/2}}^{silicate}}\right] \quad (4)$$

If the valence n is correctly determined, K_D is independent of fo_2. If the terms on the right of (4) can be considered constants over the ranges of composition considered, then K_D can be parameterised for use in further calculations purely as a function of P and T. Once a correction for the effect of carbon has been made (see Appendix), it is reasonable to consider metal activity coefficients as constants over the range of compositions explored. Several studies have reported effects of silicate melt composition, particularly the degree of polymerisation, on siderophile element partitioning and have parameterised this as a function of nbo/t (non-bridging oxygen per tetrahedrally coordinated cations) (e.g. Jana and Walker, 1997; O'Neill and Eggins, 2002). However, as the melt compositions we employ are all MgO-rich and depolymerised we have ignored this effect. In one set of experiments performed at 6 GPa in MgO capsules, unusually MgO-rich silicate melt compositions were encountered with an average Mg/Si (molar) ratio of 2.0 (see Table 2). The elevated MgO concentration in these silicate melts clearly decreased the partition coefficients of some highly charged cations, such as Nb, Ta, Si and to a lesser extent of V, and we therefore excluded these results (samples V346, V366, V365, V367) from the data regression for these elements. Our study shows, therefore, that there are advantages and disadvantages in the use of both graphite and MgO capsules that can only be appreciated through comparisons between data obtained using both types.

Values of K_D for each element were fit using the following equation (Righter et al., 1997; Righter and Drake, 2003):

$$\log K_D^M(P,T) = a + \frac{b}{T} + \frac{cP}{T} \quad (5)$$

where a, b and c are constants, T is in K and P in GPa. Wade and Wood (2005) employed 1 bar data on the free energy of formation of the oxides to calculate equilibrium coefficients for the end-member exchange reactions that could be used to constrain the temperature-dependence of K_D (Chase et al., 1998; Barin et al., 1989). This required values for $\gamma_M^{0,metal}$, the activity coefficient of metal M infinitely diluted in Fe-rich metal, which as well shows a $1/T$ dependence, from the literature. We have similarly employed such thermodynamic data to constrain the temperature-dependences of K_D for some elements for which appropriate data are available. Details of the data and the regression procedure employed for each element are outlined below and regression values are reported in Table 5.

4.1.1. Silicon

When our results and literature data are compared with the temperature trend from free energy data (Fig. 3), a negative effect of pressure on $\log K_D^{Si}$ is indicated. This is in contrast to a number of previous studies that have argued for an increase in the Si content of Fe-metal with increasing pressure, at least within the pressure range of the upper mantle (Ito et al., 1995; Gessmann et al., 2001; Malavergne et al., 2004; Wade and Wood, 2005). However, most of these earlier studies examined partitioning between Fe-metal and silicate minerals or ferropericlase rather than silicate melts. In order to have data from a broader pressure range for regression we included experimental results from Takafuji et al. (2005), who equilibrated liquid Fe-metal and (Mg,Fe)SiO_3–perovskite (MgSi–Pv) in a diamond anvil

Table 5
Regression coefficients to describe log K_D[a].

	n[b]	No.[c]	a	±σ	b	±σ[d]	c	±σ
Si	4^+	23	2.98	0.02	−15,934		—[e]	
Ta	5^+	17	0.84	0.09	−13,806		−101	15
Nb	5^+	8	2.66	0.11	−14,032		−199	16
V	3^+	19	−0.48	0.38	−5063	894		
Cr	2^+	30	−0.17	0.13	−2730	312		
Mn	2^+	20	0.54	0.05	−7142		52	9
Ga	2^+	19	0.52	0.45	−514	914	−78	13
In	1^+	16	1.03	0.30	302	621	−106	10
Zn	2^+	17	−0.30	0.36	−1574	739	−51	12

[a] All regression coefficients according to Eq. (5) except for Si (see Footnote e).
[b] Valence state of the element in the silicate liquid.
[c] Number of experimental data points used for regression.
[d] Errors are given as standard deviations from the least square fit; where no value is listed b was fixed to the one derived from the free energy data.
[e] Regression term used for Si: $\log K_D = a + b/T + (c_1P + c_2P^2 + c_3P^3)/T$ with c_1: −155 ± 25; c_2: 2.26 ± 0.84; c_3: −0.011 ± 0.007.

cell at P–T conditions of 25–97 GPa and 2500–3150 K. High pressure (24–35 GPa) silicate melt-perovskite partitioning data (Trønnes and Frost, 2002; Ito et al., 2004) indicate that the metal–silicate K_D^{Si} estimated from metal–perovskite partitioning is likely to be very close to that involving silicate melt. For Si, we used a third order polynomial to fit the effect of pressure observed with our data because its influence appears to become weaker as P increases.

4.1.2. Tantalum and niobium

For both Ta and Nb, negative pressure-trends are observed (Figs. 3 and 4), with a much stronger trend for Nb than for Ta. The temperature trends for both elements are based on the free energy data of the 5^+ oxides but are corrected for the temperature-dependence of the respective $\gamma_M^{0,metal}$ values. For fitting the pressure trends, we used the linear relationship of Eq. (5) in both cases, including data of Wade and Wood (2001) and additionally of Wade and Wood (2005) for Nb. In Fig. 3 we have plotted the result of a Ta-partitioning experiment of Rammensee et al. (1983), performed in an alumina capsule at 1 bar. In general this is consistent with the trend defined by the high pressure data, though it might indicate a stronger pressure-dependence at $P < 2$ GPa. As discussed above, 6 GPa data collected in MgO capsules give low K_D values for Nb, most likely because of the very high MgO contents of the silicate melts, whereas K_D values obtained using graphite capsules are too high. Therefore, all 6 GPa data for Nb were excluded from the fit. However, these data (the results from graphite-capsule experiments uncorrected for the effect of

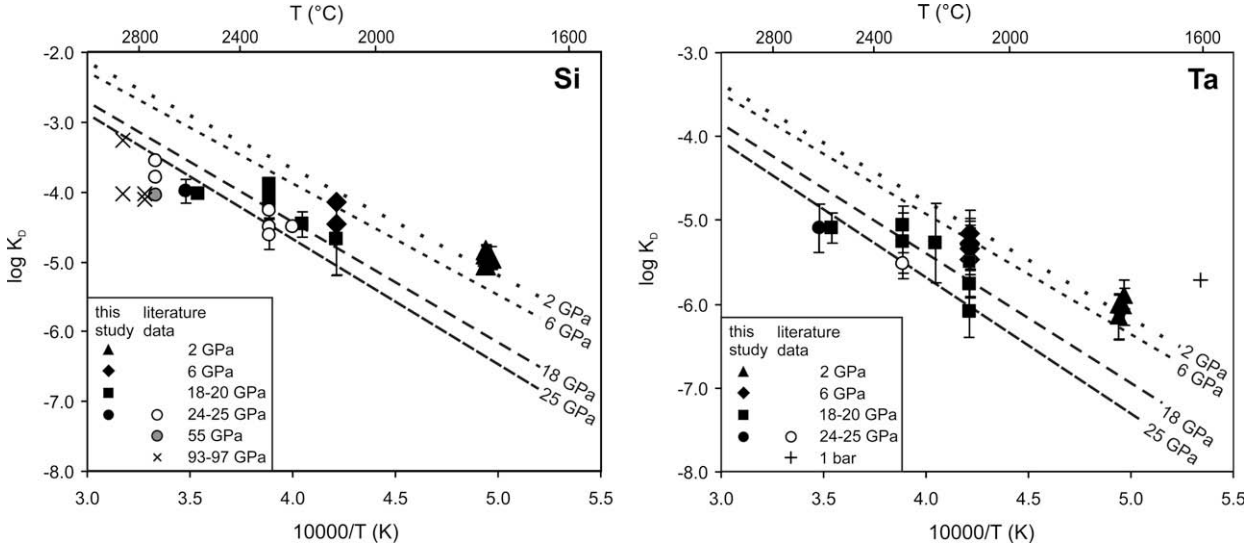

Fig. 3. The logarithmic values of the exchange coefficients (K_D) of Si and Ta plotted as a function of inverse temperature (10,000/T). Filled black symbols are data from this study. Data from the literature include for Si: 25 GPa — Wade and Wood (2001, 2005); 25–97 GPa — metal–MgSi–Pv partitioning experiments of Takafuji et al. (2005). For Ta: 1 bar (alumina capsule) — Rammensee et al. (1983); 25 GPa from Wade and Wood (2001). Where no error bars are shown the uncertainties do not exceed the symbol size. The lines show the pressure–temperature trends obtained from data regression for the pressures as indicated (see text).

C (for details see Appendix)) are plotted on Fig. 4 to illustrate the contrasting effects of the respective capsule materials. The same effects also apply to the Ta data at 6 GPa, but in this case the graphite-capsule results could be corrected for the carbon effect, and were thus included in the data regression.

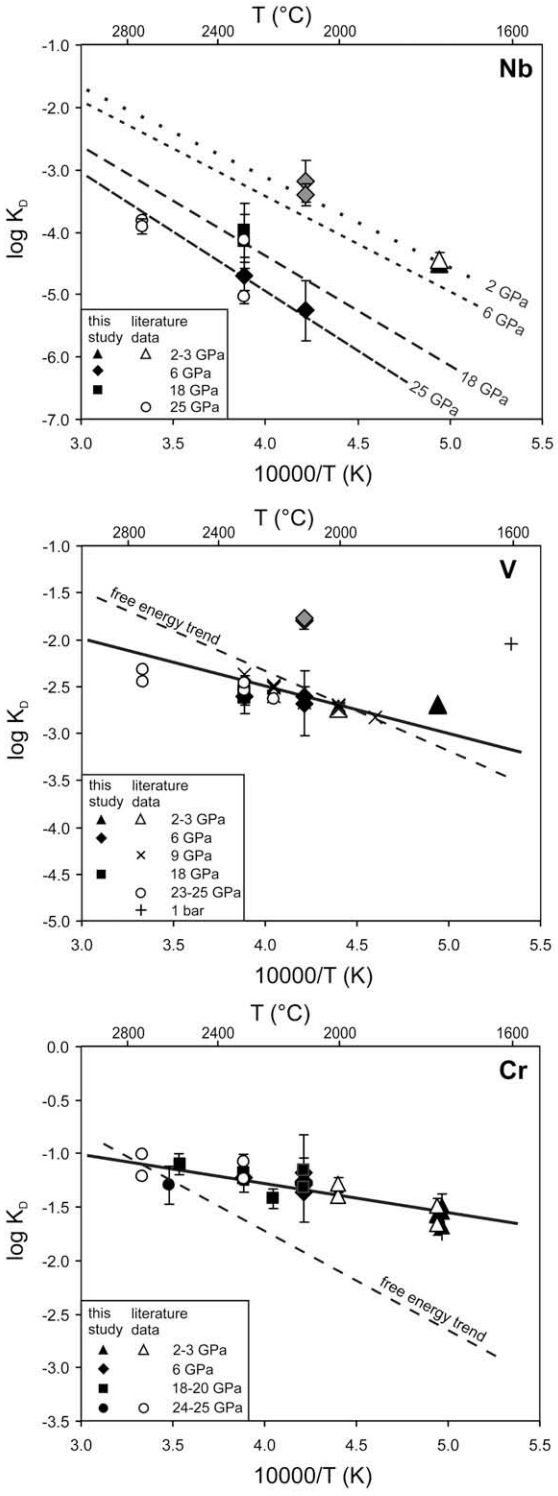

Fig. 4. The logarithmic values of the exchange coefficients (K_D) of Nb, V and Cr plotted as a function of inverse temperature (10,000/T). Filled black symbols are data from this study. Data from the literature include for Nb: 2.5 and 25 GPa from Wade and Wood (2001, 2005). For V: 1 bar experiment (alumina capsule) — Rammensee et al. (1983); 3 GPa — Chabot and Agee (2003); 9 and 23 GPa — corrected data from metal–MgO partitioning experiments (see text) — Gessmann and Rubie (2000); 25 GPa — Wade and Wood (2001, 2005). For Cr: 2.5 GPa —Wade and Wood (2001); 3 GPa — Chabot and Agee (2003); 25 GPa — Wade and Wood (2001, 2005). Where no error bars are shown the uncertainties do not exceed the symbol size. For V and Cr the thick solid lines correspond to the pressure-independent best-fit equation as explained in the text. The dashed lines indicate the respective slope of the free energy trends of V_2O_3 and Cr_2O_3 (corrected for $\gamma_M^{0,metal}(T)$) which are too steep to fit the T slopes observed for our datasets. For Nb the lines show the pressure–temperature trends obtained from data regression (see text) for the pressures as indicated. For discussion of the deviation of some of the V and all of the Nb data at 6 GPa (filled grey symbols — data obtained from graphite capsules) from the respective P trends see text.

4.1.3. Vanadium

The 1 bar free energy temperature trend of V_2O_3 is much steeper than what is observed for our experimental dataset (Fig. 4). For determining the K_D trend we therefore included data on metal–ferropericlase partitioning, which we corrected using a silicate melt–ferropericlase exchange coefficient determined from our data. Literature data on metal–ferropericlase partitioning extends from 2073 to 2673 K, which is an excellent range over which to constrain the temperature-dependence (Gessmann and Rubie, 1998; Gessmann et al., 1999). Our data for the metal–ferropericlase partitioning of V show a weak positive dependence on pressure, which is in good agreement with the results of Gessmann and Rubie (2000). Additionally, the silicate–ferropericlase K_D obtained from our results also shows a slight positive, linear dependence on P, which implies a minimal pressure-dependence of metal–silicate melt partitioning. The fitted data set including literature data (1 bar — Rammensee et al., 1983; 3 GPa — Chabot and Agee, 2003, corrected values at 9 and 23 GPa — Gessmann and Rubie, 2000; 25 GPa — Wade and Wood, 2005) reveals no significant pressure-dependence in the range 6–25 GPa. Inconsistencies with low pressure data (<6 GPa), particularly at 1 bar, may indicate a stronger P-dependence at low pressure, similar to the low P partitioning behaviour recently reported for Ni and Co by Kegler et al. (2008). As there are not enough experimental data for V to support this possibility, we have neglected it in our regression. As is the case for Nb, the uncorrected 6 GPa data from graphite capsules are shown in Fig. 4 for comparison with the results from MgO capsules, illustrating the large effect of C on V partitioning (see Appendix).

4.1.4. Chromium

The strong temperature-dependence predicted from the free energy data for Cr_2O_3 does not satisfy the observed experimental trend, which reflects the presence of Cr^{2+} in the silicate melts (Fig. 4). Therefore, the temperature trend

was obtained by fitting an extended data set employing experimental results at 2.5–3 and 25 GPa from the literature (Wade and Wood, 2001, 2005; Chabot and Agee, 2003) where Cr was found to be in the 2^+ state. There may be a slight negative pressure-dependence to log K_D^{Cr} but this is within the uncertainties of the data, and was neglected in the regression.

4.1.5. Manganese

As graphite capsule data at both 2 and 6 GPa lie within the range of uncertainties of the MgO capsule results we also included literature data obtained at 2 and 7.7 GPa in graphite capsules (Wade and Wood, 2005; Corgne et al., 2008), as well as other literature data from MgO capsules at 2–3 and 25 GPa (Kilburn and Wood, 1997; Wade and Wood, 2001; Chabot and Agee, 2003). Our graphite capsule data at 20 GPa, 2373 K show a strong shift towards higher K_D values (Fig. 5) and were therefore not included in the data regression. For fitting the temperature trend we started from the free energy data for MnO and corrected for the effect of temperature on $\gamma_{Mn}^{0,metal}$. The slope for the derived trend is in good agreement with the temperature-dependence of the metal–ferropericlase K_D of our study and of Gessmann and Rubie (2000). Consequently, the silicate–ferropericlase K_D for Mn is considered to be constant with pressure. After correcting all metal–silicate K_D data to

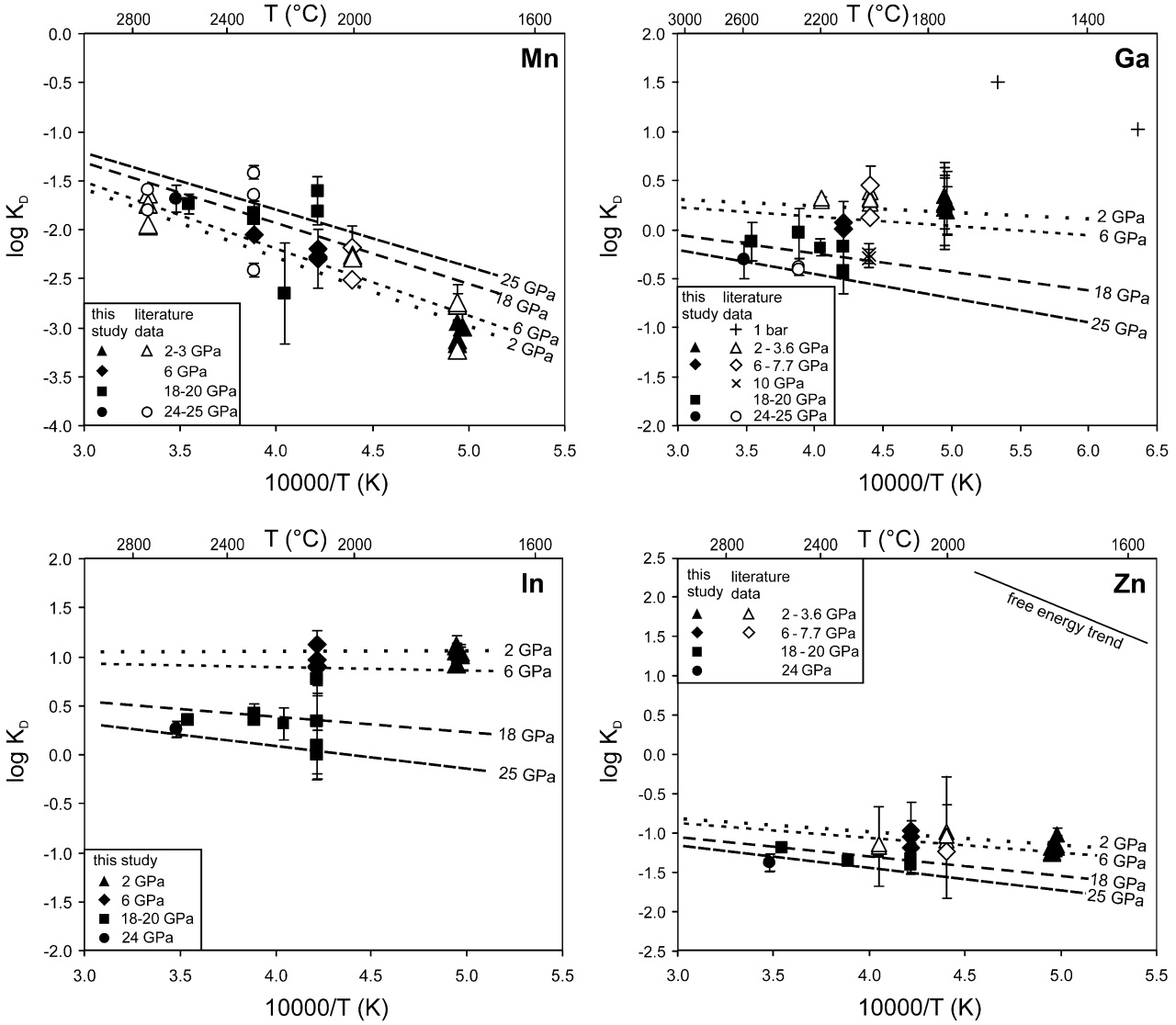

Fig. 5. The logarithmic values of the exchange coefficients (K_D) of Mn, Ga, In and Zn plotted as a function of inverse temperature (10,000/T). Filled black symbols are data from this study. Data from the literature include for Mn: 2.5 GPa — Kilburn and Wood (1997); 3 GPa — Chabot and Agee (2003); 7.7 GPa Corgne et al. (2008), 2–2.5 and 25 GPa — Wade and Wood (2001, 2005). For Ga: 1 bar (alumina capsule) — Schmitt et al. (1989); 3.6 and 7.7 GPa Corgne et al. (2008), 10 GPa — Hillgren et al. (1996); 25 GPa — Wade and Wood (2001). For Zn: 3.6 and 7.7 GPa Corgne et al. (2008), Where no error bars are shown the uncertainties do not exceed the symbol size. The lines show the pressure–temperature trends obtained from data regression (see text) for the pressures as indicated. For Zn the thin solid line indicates the free energy trend of ZnO (without $\gamma_M^{0,metal}$ correction) which does not match the T dependence observed for our dataset.

2273 K, a positive pressure effect can be observed which gets weaker towards higher pressures and increases log K_D by 0.45 from 2 to 18 GPa. For defining the K_D trend we considered a linear pressure-dependence only. A weak positive pressure-trend has also been derived by Ohtani et al. (1997) and Corgne et al. (2008), although in both cases from graphite-capsule results, whereas Chabot and Agee (2003) could not detect a clear P-dependence between 3 and 14 GPa, probably as a result of the limited pressure range studied.

4.1.6. Gallium, indium and zinc

There are no free energy data available for GaO or In_2O for defining K_D temperature trends, and for ZnO we find the temperature-dependence of the 1 bar free energy data (Barin et al., 1989) to be inconsistent with our data set (see Fig. 5). All three elements were, therefore, fitted using Eq. (5) without any constraints being provided by the free energy data. In the case of Ga, we included literature data at 10 and 25 GPa (Hillgren et al., 1996; Wade and Wood, 2001) for refining our trend (Fig. 5), however, most of the previous studies of Ga partitioning employed Ni-rich (>25 wt%; Capobianco et al., 1999; Righter and Drake, 2000) metals or MgO-poor silicates (<13 wt%; Jaeger and Drake, 2000), which are not comparable to our compositions. Fig. 5 additionally shows results for Ga from graphite capsules of Corgne et al. (2008) that were corrected for the effect of C (see Appendix). No previous metal–silicate partitioning data have been presented for In and for Zn there are only data available from Corgne et al. (2008), which were included in Fig. 5 after correcting for the C effect.

Our data indicate that Ga, In and Zn become less siderophile with increasing pressure (Fig. 5) with the pressure effect for In being about twice as large as that for Zn. If 1 bar partitioning data of Schmitt et al. (1989) are considered it is possible that a stronger P effect on Ga occurs at $P < 2$ GPa. The influence of temperature on the partitioning behaviour of all three elements is rather small, especially for In, which is consistent with the 1^+ valence state that we have derived.

4.2. The effect of S

Sulphur would have been present in core-forming Fe-rich liquids and consequently its effect on element partitioning needs to be considered. Therefore, S-bearing experiments were performed at 2 GPa and 2023 K, 9 GPa and 2373 K and 18 GPa and 2573 K in MgO capsules. The quenched metals of these samples contain 26.4, 10.5 and 7.6 wt% S, respectively, which corresponds to mole fractions of 0.39, 0.17 and 0.13 (Table 2). In Fig. 6, the K_D values for V, Nb, Mn, Ga, In, Zn, Cr and Ta, determined from these samples, are plotted as a function of X_S and are compared to results obtained from S-free experiments run at the same or similar P–T conditions including data from the literature (Chabot and Agee, 2003; Wood et al., 2008b). In general, we observe that the presence of S in the metal causes an increase in K_D for V, Cr, Ta and Mn whereas it decreases K_D for Ga. A very small increase in K_D for Nb with S content is consistently observed at each set of conditions but the increase is smaller than the uncertainties. There is no significant effect of S on In and Zn. The effect of S generally becomes weaker as pressure and temperature increase, especially in the case of Mn. However, the maximum change of K_D does not exceed 1–2 orders of magnitude even at $X_S = 0.4$. In general our results are consistent with literature data (Fig. 6). The relatively high K_D's for Mn at 3 GPa from Chabot and Agee (2003) are a consequence of the higher temperatures under which these experiments were performed compared with our 2 GPa experiments.

5. IMPLICATIONS FOR CORE FORMATION

Having defined the pressure, temperature (see above) and oxygen fugacity (see Appendix) dependences of the metal–silicate partition coefficients of a range of elements, we use these to test and further constrain core-formation models. The partition coefficients will determine the chemical compositions of the metallic core and silicate mantle that form by differentiation of a planetary body. The final core-mantle partition coefficient of element M for the Earth, $D^{core\text{-}mantle}$ (M), is defined by the core to mantle concentration ratio and can be estimated by a mass balance calculation that is based on the mantle concentration of element M (e.g. McDonough and Sun, 1995; Palme and O'Neill, 2003), the assumption of a chondritic bulk composition for the Earth and a core mass fraction of 0.32. Traditionally, $D^{core\text{-}mantle}$ (M) values have been compared with experimentally-determined partition coefficients to define a single set of P–T conditions of metal–silicate equilibration. In reality, core formation was clearly an on-going process that likely took place over much of the Earth's accretion history. Therefore, in models involving high-pressure metal–silicate equilibration (e.g. in a series of impact-induced magma oceans), equilibration pressures must increase progressively as the Earth accretes (Wade and Wood, 2005; Rubie et al., 2007). For simplicity, we take here the traditional approach and constrain "effective" equilibration pressures — which can be considered as averaged values that are the net result of on-going core-mantle differentiation over a range of conditions during accretion. It is therefore not our goal to develop a detailed model for core-mantle equilibration but to provide solid evidence that certain element ratios in the Earth's mantle must result from metal–silicate equilibration at high pressures and could not have been derived through heterogeneous accretion processes involving only low-pressure (<1 GPa) equilibration. Experimental observations have been used to imply that the mantle Ni/Co ratio may result from high-pressure metal–silicate equilibration (Li and Agee, 1996; Righter et al., 1997) however this observation does not by itself exclude low pressure heterogeneous accretion models (Wänke, 1981; O'Neill, 1991) that are just as successful in reproducing this ratio.

5.1. The relative behaviour of Ta and Si

Ta is present in the bulk silicate Earth in chondritic relative abundance (McDonough and Sun, 1995; Rudnick

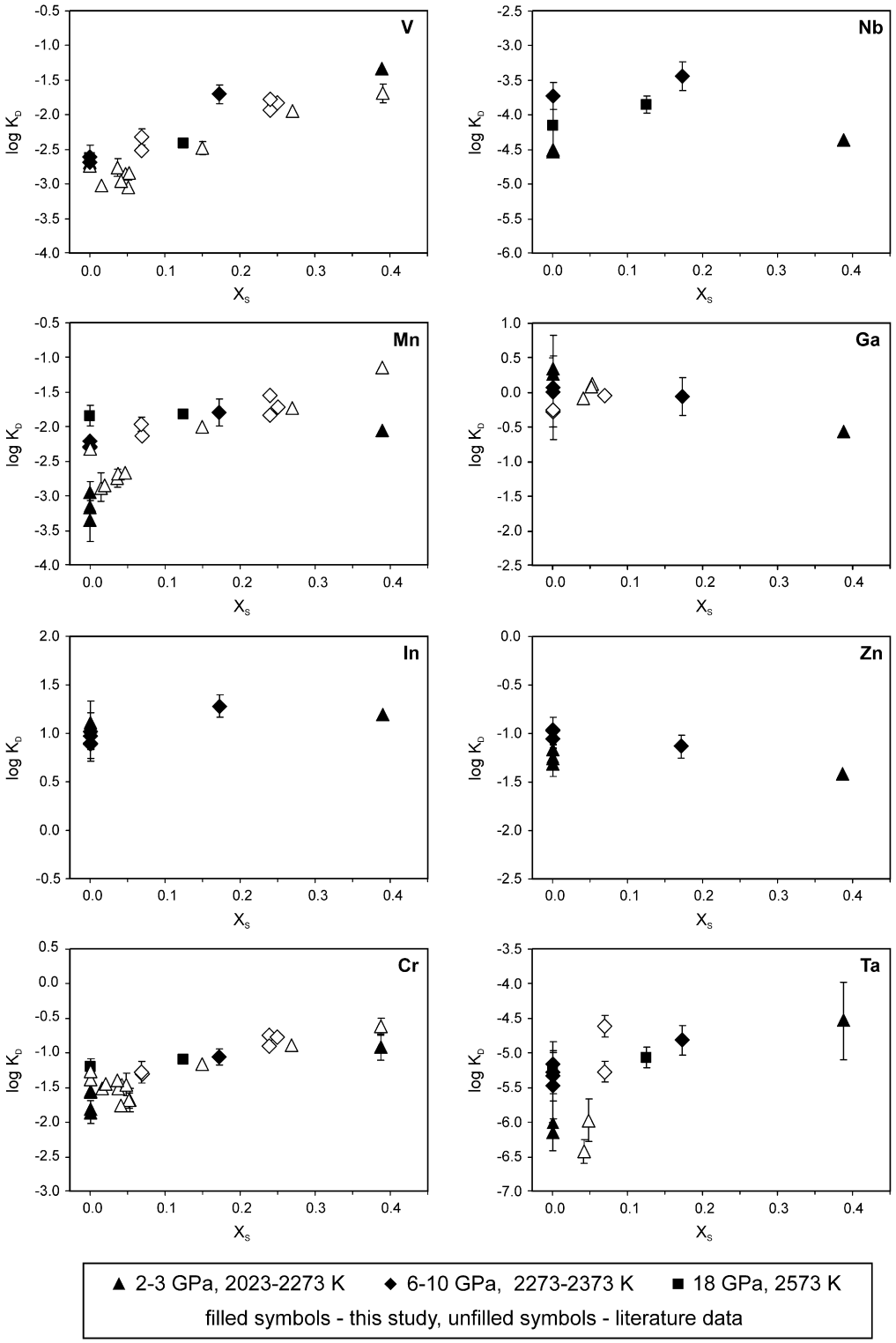

Fig. 6. Influence of S on the exchange coefficients (K_D) of V, Nb, Mn, Ga, In, Zn, Cr and Ta displayed as a function of mol fraction of S in the metal (X_S). Filled symbols are results from this study (2 GPa, 2023 K; 6 GPa, 2373 K; 9 GPa, 2373 K, 18 GPa, 2573 K). Literature data (unfilled symbols) include: 3, 6 and 10 GPa all at 2273 K — Chabot and Agee (2003); 2.5 GPa, 2023 K and 8 GPa, 2273 K — Wood et al. (2008b).

et al., 2000) but would become sidereophile at very low oxygen fugacities. Any core-formation model that requires conditions sufficiently reducing to deplete significant Ta from the mantle can therefore be excluded. Our results indicate

that Ta is less siderophile than Si, Nb or V at all likely core formation conditions. It therefore provides no constraints on whether, for example, Si could have entered the core. The extraction of a significant amount of U into the core by liquid metal–liquid silicate partitioning (Wheeler et al., 2006; Malavergne et al., 2007) can be excluded, however, on the grounds that it requires oxygen fugacities below ΔIW-5 which would have led to a strong depletion of Ta from the mantle.

5.2. The relative behaviour of V and Nb

The partitioning of the weakly-siderophile element V, with $D^{core\text{-}mantle}$ ~1.6–2.2, provides an important constraint on the conditions of core formation. As discussed above, pressure has a negligible effect on the metal–silicate partitioning of V (Fig. 4). In order to make V sufficiently siderophile to explain its observed degree of depletion from the mantle, previous models have proposed metal–silicate equilibration under either (a) very reducing conditions (Wänke, 1981; O'Neill, 1991; Wade and Wood, 2005), or (b) very high temperatures (e.g. 700 K above the peridotite liquidus) (Gessmann and Rubie, 2000; Chabot and Agee, 2003), although the latter may not be physically realistic. On the other hand, Nb was lithophile, or at the very least only slightly siderophile (Wade and Wood, 2001), during core formation, with $D^{core\text{-}mantle}$ ~0–0.9. In contrast to V, pressure has a strong effect on the partitioning of Nb and the effect of temperature is also relatively strong (Fig. 4). Consequently, the behaviour of these two elements can be used to constrain a minimum average pressure for the conditions of core formation. For example, at 2 GPa and 2973 K, their respective K_D values are almost identical and therefore core formation at such conditions cannot explain their contrasting (siderophile vs. lithophile) behaviour in the Earth.

We use our newly-derived partitioning data (Table 5) to determine conditions of core formation under which Nb would be lithophile and V would be siderophile, taking the respective estimated values of $D^{core\text{-}mantle}$ as constraints. To do this, we first assume (following Wade and Wood, 2005) that temperatures of metal–silicate equilibration during core formation were close to the peridotite liquidus, as defined by Herzberg and Zhang (1996) and Zerr et al. (1998). We then calculate the oxygen fugacities (ΔIW) along the peridotite liquidus that would be required to produce the estimated $D^{core\text{-}mantle}$ value for V (1.65). Finally we calculate the partition coefficient of Nb as a function of pressure at temperatures along the peridotite liquidus using the same oxygen fugacities defined in the previous step (Fig. 7). Because some proportion of metal might equilibrate at temperatures above the liquidus in a magma ocean during core formation (Rubie et al., 2003) and also because of uncertainties in the high-pressure liquidus determination, we have also performed the calculation at $T = T_{liquidus} + 200$ K (dashed curve in Fig. 7).

At low pressures and f_{O2} conditions necessary to achieve $D^{core\text{-}mantle}$ (V) = 1.65, calculated values of D (Nb) exceed, by at least an order of magnitude, the upper limiting value of 0.9 that is estimated for the Earth (based on a 30% depletion using the values of Münker et al., 2003) — see dashed horizontal line in Fig. 7. At higher pressures, D (Nb) decreases but the value of 0.9 is reached only at $P > 25$ GPa. If the temperature is 200 K above the peridotite liquidus, the pressure would have to be at least 35 GPa in order for the constraints for V and Nb to be fulfilled

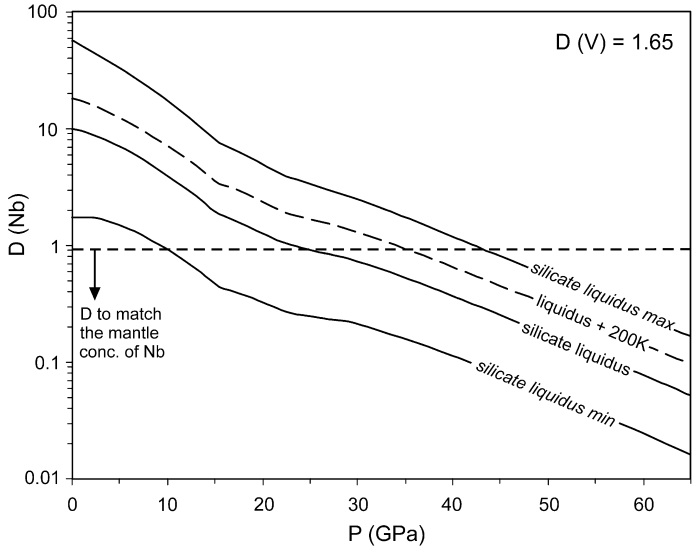

Fig. 7. The partition coefficient D of Nb as a function of pressure calculated for oxygen fugacities where the partition coefficient D for V matches the observed present day mantle abundance (D(V) = 1.65). The temperature is fixed along the peridotite liquidus (solid line) and 200 K above it (dashed line), as determined by Herzberg and Zhang (1996) and Zerr et al. (1998). The required D(Nb) for the core/mantle ratio (⩽0.9) is indicated with the horizontal line. The uncertainty range for the calculation at the liquidus is indicated with the two solid curves at the top and the bottom and is based on the variations of D(Nb) due to the uncertainties of each regression coefficient of the K_D fits for both Nb and V (see text).

simultaneously. If the value of $D^{core\text{-}mantle}$ (Nb) is significantly lower than 0.9, the pressure of metal–silicate equilibration could be as high as 50–60 GPa (Fig. 7).

Extrapolating our data set using the derived regression trends involves some uncertainty. To explore its range we have calculated the variations of D (Nb) due to each regression coefficient of the K_D fits for both Nb and V and have added or subtracted the square root of the sum of the variations in quadrature. The upper and lower limits for the D (Nb) P–T trend calculated with this method for conditions at the peridotite liquidus are shown in Fig. 7. Even though the uncertainty range is broad, it shows that even in the lowest case, pressures of at least 10 GPa are needed to produce the mantle concentrations of both V and Nb, whereas 45 GPa would be required considering the upper limit of the uncertainty. This observation strongly supports core formation scenarios that postulate metal–silicate equilibration at high pressures and, therefore, models involving a deep magma ocean that could have provided such conditions.

The results of Fig. 7 provide a robust constraint on the lower-pressure limit of metal–silicate equilibration during formation of the Earth's core. Heterogeneous core-formation models that postulate an early phase of metal–silicate equilibration in small bodies at very reducing conditions and low pressures (e.g. $\leqslant$1 GPa), even though successful in explaining the depletions of siderophile and weakly-siderophile elements such as V from the mantle, would have resulted in a strong depletion of Nb. Based on our data, models of low-pressure core formation during heterogeneous accretion like those proposed by Wänke (1981) and O'Neill (1991), can therefore be excluded. Our data are in general agreement with the model of Wade and Wood (2005) in that the oxygen fugacity at which the V depletion of the mantle occurred must have been lower than that at which the main siderophile element concentrations in the mantle (e.g. Fe, Ni, Co) were established. Thus the implication is not only that high pressure and temperature equilibration occurred but also that an increase in the oxygen fugacity of metal–silicate equilibration must have also occurred with time during core formation.

5.3. The relative behaviour of Ga and Mn

In order to further constrain core-formation models, we consider the relative behaviour of selected pairs of elements that show little or no relative fractionation in the Earth's mantle. The elements Mn and Ga constitute one such example (Fig. 1) and are especially useful because of the opposite effects of pressure on their metal–silicate partitioning (Fig. 5). Both elements are considered to be moderately to weakly siderophile but are also volatile to different extents. No matter which processes contributed to their present mantle depletions, the sum of the processes involved resulted in these elements having almost the same degree of depletion in the mantle relative to CI chondrite. Therefore, we can exclude conditions of metal–silicate equilibration that would strongly fractionate Mn and Ga in a way that it could not be reversed by their different volatilities.

In Fig. 8 we show the ratio of the metal–silicate partition coefficients of Ga and Mn calculated over the pressure range 1–80 GPa, again with temperatures fixed to the peridotite liquidus (solid line). As both elements have a 2^+ valence state (see Table 5 and Appendix, Fig. A1), these calculations are independent of oxygen fugacity. The dashed horizontal line indicates the D(Ga)/D(Mn) ratio of the Earth that needs to be matched to achieve zero fractionation. This ratio is a theoretical value, treating both elements as refractory and regarding depletion by metal–silicate partitioning only. In reality, with any volatile depletion having occurred prior to core formation, the ratio must fall below this line, as Ga with its lower condensation

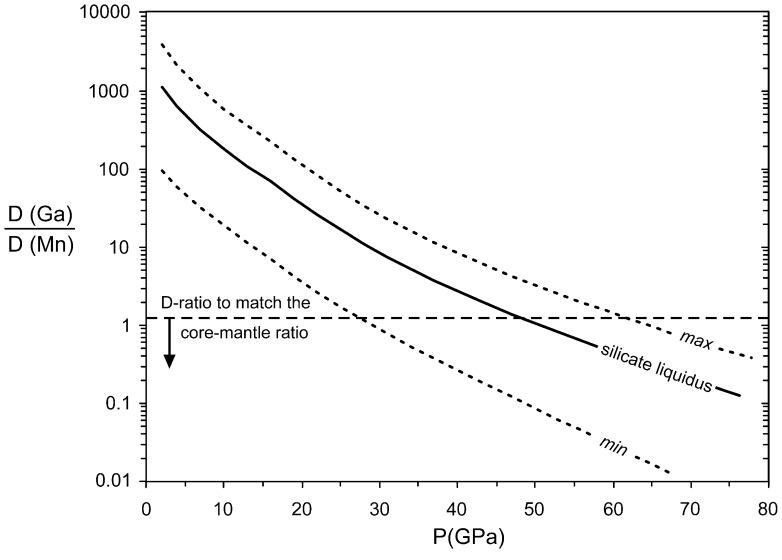

Fig. 8. The partition coefficient of Ga relative to that of Mn as a function of pressure with temperature fixed along the peridotite liquidus (solid line). The maximum value of the D(Ga–Mn) ratio for the mantle (= 1.2) is indicated by the dashed horizontal line, representing depletion by metal–silicate partitioning only. The uncertainty range is indicated with the two dashed curves and is derived from error propagation of the uncertainties of each regression coefficient of the K_D fits for both Ga and Mn (see text, Section 5.2).

temperature would have been affected to a greater extent than Mn.

At moderate pressures, e.g. ~20 GPa (the minimum pressure estimate based on Nb partitioning), Ga would be much more siderophile and would therefore be depleted from the mantle to a much greater extent than Mn. With increasing pressure, the ratio D(Ga)/D(Mn) decreases strongly as a result of D(Mn) having a positive and D(Ga) a negative pressure-dependence, as well as D(Mn) having the stronger temperature-dependence (Fig. 5). A pressure of at least 50 GPa is required for the ratio to reach a value where zero fractionation of the two elements in the mantle would occur as a consequence of core formation. Based on error propagation (performed in the same way as described for Nb and V in Section 5.2), the possible range for this minimum pressure estimate is 30–60 GPa (dotted curves in Fig. 8). However, because Ga is more volatile than Mn (Fig. 1), the equilibration pressure could be significantly greater than 50 GPa. Thus our results on the partitioning behaviour of these two elements also unequivocally support models of core formation that involve metal–silicate equilibration at very high pressures.

As discussed above the presence of light alloying components such as S or C in the metal phase could change the relative partitioning behaviour of Mn and Ga. We have observed that the partition coefficient of Ga decreases in the presence of both S and C while that of Mn increases with X_S and is barely affected by C (Figs. 6 and A1; Table A2). However, in order to significantly change the Ga–Mn partition coefficient ratio at any P–T condition, the concentrations of S and C in the metal would have to be very high ($X_S > 0.3$, $X_C > 0.15$), which is unrealistic for the Earth's core.

5.4. The relative behaviour of In, Zn and Pb

In and Zn also show little or no fractionation in the Earth's mantle despite the condensation temperature of In being almost 200 K lower than that of Zn (Fig. 1). We can therefore determine their relative metal–silicate partitioning behaviour to constrain core formation conditions, as we have done above for Ga and Mn. Because the valence states are different (1^+ for In and 2^+ for Zn), the ratio of the metal–silicate partition coefficients for In and Zn depends on oxygen fugacity as well as P and T. The effect of fo_2 is shown in Fig. 9 for various pressures and with temperature fixed to the peridotite liquidus. As for Ga and Mn, we show the upper limit of the ratio D(In)/D(Zn) for the Earth in Fig. 9, which would be the fictive value if these elements were fully refractory and depleted only by metal–silicate partitioning during core formation. If volatility has affected their abundances, which is almost certainly the case, the required ratio is even lower.

The likely fo_2 range during core formation was ΔIW-4 to ΔIW-2 (e.g. Wade and Wood, 2005). Fig. 9 shows that over this fo_2 range, metal–silicate equilibration pressures of at least 40 GPa are required in order to produce the estimated D(In)/D(Zn) ratio for the Earth. In the case of low-pressure equilibration (<1 GPa), as proposed by Wänke (1981), a fo_2 of ΔIW-8 (or lower) would be required to produce the mantle concentrations of In and Zn, which would have caused other weakly-siderophile elements, such as V and Nb, to be removed completely from the mantle.

A number of studies have concluded that metal–silicate equilibration occurred in a magma ocean at conditions of 30–60 GPa, 2000–4000 K and $fo_2 \sim$ ΔIW-2 (e.g. Gessmann and Rubie, 2000; Li and Agee, 2001; Chabot et al., 2005).

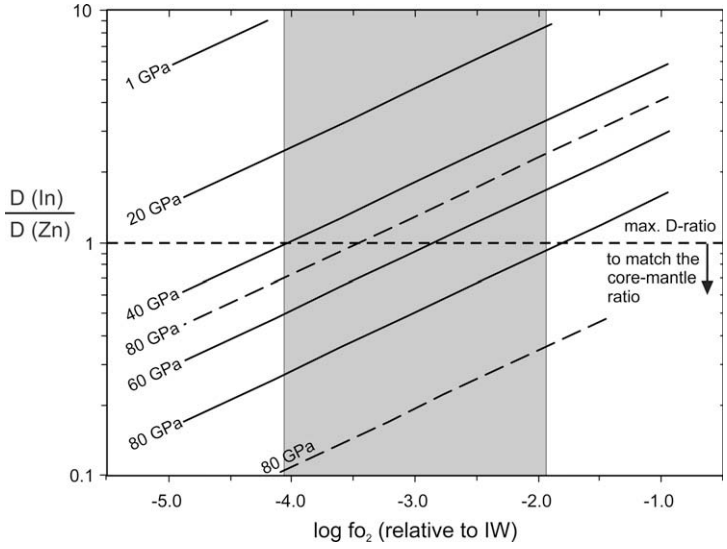

Fig. 9. The ratio of the partition coefficient D of In (1^+) relative to that of Zn (2^+) as a function of oxygen fugacity (expressed relative to the iron-wüstite buffer, ΔIW), at different pressures. At each pressure the temperature is fixed at the peridotite liquidus. For the curve at 80 GPa, the uncertainty range based on the error propagation of the uncertainties of the In- and Zn-K_D regression coefficients (see text, Section 5.2) is shown by the dashed lines. The maximum D ratio for the two elements in the Earth's mantle is set to 1 (dashed line) which is the upper limit if both elements were depleted from the mantle by core formation only. Considering volatility, the value must be <1. The grey area indicates the range of oxygen fugacities proposed in various core-formation models, the upper end being consistent with the current FeO content of the mantle.

At this oxygen fugacity, a pressure >80 GPa would have been necessary to produce the observed concentrations of In and Zn in the mantle (Fig. 9). Even in models where the equilibration pressure progressively increases and fo_2 starts at about ΔIW-4 and increases subsequently during accretion (Wade and Wood, 2005; Rubie and Frost, 2007), very reduced conditions would have had to persist over much of the accretional history, even if the final equilibration pressures reached 60–80 GPa.

When regressing the In and Zn data all three parameters were free and as the number of experiments for both elements is limited, the uncertainty on our prediction of their D ratios is relatively large. In Fig. 9 the uncertainty range (determined by error propagation on calculating both K_D values as described in Section 5.2) is shown for the curve determined at 80 GPa. However, even at the very lower limit, $P > 20$ GPa at conditions of ΔIW-4 are required to obtain an Earth-like In/Zn ratio, even without considering the likely initial differences due to volatility which would drive the required equilibration conditions to even higher pressures. Additionally, for In and Zn we found no significant effect on the partitioning behaviour by the presence of S in the alloy (Fig. 6). In contrast, C does reduce the partition coefficient of both elements (Fig. A1; Table A2), but as the degree of change is very similar for both elements, this would not affect their relative behaviour. Therefore, the partitioning behaviour of these two elements provides further support that metal–silicate equilibration cannot have occurred at low pressure during formation of the Earth's core.

Another revealing comparison is that between In and Pb which share an almost identical 50% condensation temperature. Pb is more depleted than In from the mantle which has been attributed to the extraction of Pb but not In into the core (Yi et al., 2000). However, comparing our data for In with that for Pb from Wood et al. (2008a) indicates that metal–silicate equilibration in a magma ocean at $P < 15$ GPa should deplete In to a much greater extent than Pb. It is only above 20 GPa that Pb could be fractionated from In to provide the observed mantle concentrations. The effect of pressure on Pb metal–silicate partitioning is not yet well constrained but seems to be negligible (Wood et al., 2008a). And even though Pb is strongly chalcophile, the K_D for In in S-rich Fe-liquids (~30 wt% S), e.g. at 2 GPa and 1750 °C is approximately 6 times that of Pb. Therefore, it is difficult to explain the depletion of Pb relative to In by the separation of a late-stage sulphide-rich melt, unless, as proposed by Wood et al. (2008a), crystallisation of silicate minerals had previously concentrated Pb within layers of silicate partial melt. If the mantle concentration of these two volatile elements was set by Fe-rich metal–silicate equilibration, the partitioning data available at present again call for high pressure conditions in a magma ocean.

5.5. Partitioning behaviour of volatile elements

Previous studies have identified a depletion trend for the least depleted lithophile or very weakly siderophile, volatile elements in the Earth's mantle (Dreibus and Palme, 1996; Palme and O'Neill, 2003). The principal tendency of this volatility trend, which describes a decrease of element abundance with decreasing condensation temperature within a reduced (H_2-rich) environment, is observed in many bodies of the inner solar system, especially the carbonaceous chondrites (Humayun and Cassen, 2000; Palme and O'Neill, 2003). This has been interpreted in terms of incomplete condensation from the solar nebula, which consequently affected all precursor material that subsequently formed the planets. For the Earth this overall volatile depletion trend is prevalent to a greater extent than in any chondritic material, but it may have been overprinted or obscured to some extent by other volatile processes that were not a simple function of condensation temperature. O'Neill and Palme (2008), for example, argued that the chondritic Mn/Na ratio of the Earth's mantle is identical to that shown in a range of carbonaceous chondrites and must result from an additional nebular fractionation process that affected Mn to a greater extent that Na during the later stage of its formation.

Similarly, our metal–silicate partitioning data on the element pairs Ga–Mn and In–Zn, which also have near chondritic ratios in the Earth's mantle, indicate problems with the classical approach of assigning element depletion relative to the volatility trend simply to core formation. Ga and In should be more strongly depleted from the mantle than Mn and Zn, respectively, as a result of both volatility and core formation, unless core formation occurred at very high pressures. Core-mantle equilibration at pressures dominantly >50 GPa would have been required to render the appropriate mantle ratios of these elements, even before we consider possible effects of varying volatility. While this is possible, it is problematic for physical models as nearly complete re-equilibration of very large proto-planetary cores would be required. One way to overcome this problem would be for the Earth to have accreted from material that did not show simple element depletions as a function of volatility. If nebular fractionation processes produced material with initially very high Ga/Mn and In/Zn ratios compared to CI, this would allow much stronger depletions of Ga and In during core formation, which would then return the two element ratios to the near chondritic values of the Earth's mantle. Almost all meteorite groups, however, have Ga < Mn and In ⩽ Zn compared to CI, as expected based on nebular volatility processes (Wasson and Kallemeyn, 1988). Only enstatite chondrites exhibit CI normalised concentrations of Ga > Mn, but even then the difference does not exceed a factor of 1.4, which would not be sufficient. Therefore, unless a nebula fractionation process occurred that is not documented in known meteorites this idea can be discarded.

Alternatively, the Earth's complete inventory of volatile elements might have been delivered through a late supply of volatile enriched material, (e.g. CI), that never experienced significant core-mantle equilibration and thus preserved near chondritic Mn/Ga and In/Zn ratios. The problem here, however, is that a metallic or sulphide phase would still be required to fractionate siderophile, volatile elements such as As, Cu, Ag and Ge. It remains to be tested whether this can occur without disturbing the concentrations of Ga and In in the mantle or other siderophile element concentrations

such as Co and Ni. Certainly, our data combined with that of Wood et al. (2008a) show that this mechanism cannot explain the depletion of Pb relative to In in the mantle.

6. CONCLUSIONS

The partitioning of the lithophile and weakly-siderophile elements, Ta, Nb, V, Cr, Si, Mn, Ga, In and Zn, between liquid Fe-rich metal and silicate melt (peridotitic composition) has been studied experimentally at 2–24 GPa, 2023–2873 K and oxygen fugacities of −1.3 to −4.2 log units relative to the iron-wüstite buffer. Experiments were performed using both MgO and graphite capsules. Significant amounts of C dissolve into the liquid metal phase when using graphite capsules and, for many of the elements studied, this has a large effect on the partitioning behaviour. Thermodynamic formulations are therefore required to correct the partitioning data for the effects of dissolved C. The effects of dissolved S are considerably less than those of C. The experimental results have enabled the valence state of the elements in silicate liquid to be determined and distribution coefficient (K_D) expressions have been fit to the data to determine the dependencies of partitioning on pressure and temperature.

Results for the elements studied eliminate the possibility that formation of the Earth's core involved metal–silicate equilibration only at low pressure, as proposed originally by Wänke (1981):

- For Nb to be lithophile and V to be slightly siderophile during core formation (as is the case for the Earth), average metal–silicate equilibration pressures of at least 10–40 GPa are required.
- The behaviour of the moderately-siderophile, volatile elements, Ga, Mn, In and Zn constrain metal–silicate equilibration pressures to be even higher. The elements Ga and Mn were depleted to similar extents relative to CI, and this can only be explained if equilibration pressures exceeded 30–60 GPa. The similar depletions of In and Zn would also have required comparably high pressures if set by core-mantle fractionation. Since volatility must also have played a role in fractionating these elements, even higher pressures may have been required.
- Alternative explanations for the chondritic Ga/Mn and In/Zn ratios in the mantle are either that these elements did not follow a simple volatile depletion trend in the material from which the Earth formed or that all volatile elements were delivered to the Earth at a late stage after core formation was mainly complete.
- The depletion of Pb from the mantle has been assigned to the separation of late-stage S-rich liquids to the core. Our data indicate, however, that this would also deplete In from the mantle. The relative depletion of Pb and In can only be explained by metal–silicate equilibration in a magma ocean if pressures exceeded 20 GPa.
- The possibility that the core contains U is excluded by the partitioning behaviour of Ta. For U to be siderophile it requires oxygen fugacities below IW-5 (Malavergne et al., 2007). At such conditions, the mantle would have been strongly depleted in Ta — which is not the case.

ACKNOWLEDGMENTS

We are grateful to Elizabeth Cottrell and two anonymous reviewers for their thorough, comprehensive and supportive reviews. The author U.M. gratefully acknowledges the support of the "Elitenetzwerk Bayern" graduate programme. H. Schulze is thanked for preparing the MgO single-crystal capsules.

APPENDIX 1. DETERMINATION OF OXYGEN FUGACITY

In experiments performed in MgO capsules the formation of ferropericlase at the capsule wall adjacent to the silicate melt allows the oxygen fugacity to be determined through the equilibrium:

$$\begin{array}{l} 2\,\mathrm{Fe} + \mathrm{O_2} \Longleftrightarrow 2\,\mathrm{FeO} \\ \text{metal} \qquad\quad \text{ferropericlase (fp)} \end{array} \tag{A1}$$

The equilibrium constant K for reaction (A1) is:

$$\log K_{(\mathrm{A1})} = \log\left[\frac{\left(a_{FeO}^{fp}\right)^2}{\left(a_{Fe}^{metal}\right)^2 f_{O_2}^{exp}}\right] = 2\log\left[\frac{X_{FeO}^{fp}}{X_{Fe}^{metal}}\right] + 2\log\left[\frac{\gamma_{FeO}^{fp}}{\gamma_{Fe}^{metal}}\right] - \log f_{O_2}^{exp} \tag{A2}$$

where $f_{O_2}^{exp}$ is the experimental oxygen fugacity and a, X and γ are the component activities, mole fractions and activity coefficients, respectively. The equilibrium between pure Fe metal and "FeO" defines the iron-wüstite (IW) oxygen buffer for which the equilibrium constant simplifies to:

$$\log K_{(\mathrm{A1})} = -\log f_{O_2}^{IW} \tag{A3}$$

where $\log f_{O_2}^{IW}$ is the oxygen fugacity of the IW buffer. For convenience the absolute experimental oxygen fugacity can be expressed relative to the IW buffer as

$$\Delta\mathrm{IW} = \log f_{O_2}^{exp} - \log f_{O_2}^{IW} \tag{A4}$$

Combining Eqs. (A2) and (A4) gives:

$$\Delta\mathrm{IW} = 2\log\left[\frac{X_{FeO}^{fp}}{X_{Fe}^{metal}}\right] + 2\log\left[\frac{\gamma_{FeO}^{fp}}{\gamma_{Fe}^{metal}}\right] \tag{A5}$$

For the metal alloys in experiments performed in MgO capsules (Table 2) we assume that Raoult's Law is valid whereby $\gamma_{Fe}^{metal} = 1$. However, γ_{FeO}^{fp} has been determined in high pressure and temperature experiments (Frost, 2003) and can be described with the expression:

$$\mathrm{RT}\ln\left(\gamma_{FeO}^{fp}\right) = (11{,}000 + 0.011P)\left(1 - X_{FeO}^{fp}\right)^2 \tag{A6}$$

where pressure (P) is in bar and R is the gas constant. By combining equations (A5) and (A6) we have:

$$\Delta\mathrm{IW} = 2\log\left[\frac{X_{FeO}^{fp}}{X_{Fe}^{metal}}\right] + \frac{2(11{,}000 + 0.011P)\left(1 - X_{FeO}^{fp}\right)^2}{\mathrm{RT}\ln 10} \tag{A7}$$

In experiments where ferropericlase and silicate melt coexisted we can define a Fe–Mg exchange coefficient (K_D) between oxide and melt:

$$K_D = \frac{X_{FeO}^{fp}\left(1 - X_{FeO}^{silicate}\right)}{X_{FeO}^{silicate}\left(1 - X_{FeO}^{fp}\right)} \quad \text{(A8)}$$

where $X_{FeO}^{silicate}$ and X_{FeO}^{fp} are the molar FeO/(FeO + MgO) ratios of the silicate melt and ferropericlase, respectively. Data from experiments and from the literature (Trønnes and Frost, 2002), covering a pressure range up to 24.5 GPa, indicate a slight positive pressure-dependence of K_D up to 6 GPa, although our data coverage prevents a tight constraint on this dependence. However, at and above 6 GPa, K_D appears to be constant with an average value of 0.72 ± 0.05. For lack of a better constraint, we have applied this value to all samples. This allows the calculation of a X_{FeO}^{fp} value (Eq. (A8)) to determine the oxygen fugacity (Eq. (A7)) for all experiments, even for those run in graphite capsules, based on silicate melt analyses alone ($X_{FeO}^{silicate}$). For example in sample Z442 (18 GPa, 2573 K) we measured $X_{FeO}^{silicate} = 0.027$, which with the constant $K_{D(A8)}$ results in $X_{FeO}^{fp} = 0.020$ and thus an oxygen fugacity of ΔIW-2.8 ($X_{Fe}^{metal} = 0.86$). In the same way we calculate values of $X_{FeO}^{silicate} = 0.055$, $X_{FeO}^{fp} = 0.04$ and ΔIW-2.3 ($X_{Fe}^{metal} = 0.94$) for sample V310 (6 GPa, 2373 K) run in a graphite capsule. The results obtained for ΔIW in each experiment are listed in Table 2 together with the run conditions.

APPENDIX 2. PARTITION COEFFICIENTS AND VALENCE STATE

The distribution of element M, with a valence n, between a Fe-rich liquid metal and a liquid silicate is controlled by the equilibrium

$$\mathrm{M}^{metal} + \frac{n}{4}\mathrm{O}_2 = \mathrm{MO}_{n/2}^{silicate} \quad \text{(A9)}$$

The molar partition coefficient (D) for metal M between metallic and silicate melt is:

$$D\frac{metal}{silicate}(\mathrm{M}) = \left[\frac{X_M^{metal}}{X_{MO_{n/2}}^{silicate}}\right] \quad \text{(A10)}$$

where X denotes the mole fraction of the element or oxide in the metal or melt, respectively. Positive and negative log D values indicate siderophile and lithophile behaviour, respectively. The calculated D values for Si, Ti, V, Cr, Mn, Ta, Nb, Ga, In, Zn and Fe of all samples are listed in Table A1 of the Appendix. The uncertainties are based on the standard deviation of each mole fraction and the respective error propagations on calculating D. In some samples the concentrations of Si, Ti, Ta, Mn, Ga and In were close to or below the detection limit in either the silicate or the metal phase (see Table 3), resulting in large errors for the D values.

The equilibrium constant K for reaction (A9) can be written as:

$$\log K_{(A9)} = \log\left[\frac{X_{MO_{n/2}}^{silicate}}{X_M^{metal}}\right] + \log\left[\frac{\gamma_{MO_{n/2}}^{silicate}}{\gamma_M^{metal}}\right] - \frac{n}{4}\log f_{O_2}^{exp} \quad \text{(A11)}$$

By assuming that the activity coefficients γ_M^{metal} and $\gamma_{MO_{n/2}}^{silicate}$ for the elements under investigation remain constant over the range of compositions examined and log $K_{(A9)}$ is a constant at a fixed pressure and temperature, Eq. (A11) can be rearranged to give

$$\log D\frac{metal}{silicate}(\mathrm{M}) = -\frac{n}{4}\Delta\mathrm{IW} + const. \quad \text{(A12)}$$

where ΔIW is the oxygen fugacity as defined by Eq. (A4). The valence state n of an element in the silicate liquid can then be determined using plots of log D versus log fo_2 at a constant pressure and temperature (Fig. A1).

Considering data only from MgO capsules, linear trends in Fig. A1 indicate valences in the silicate melt of 5^+ for Ta and Nb, 4^+ for Si, 3^+ for V and 2^+ for Mn, Zn and Ga. Ga was previously found to be trivalent in 1 bar partitioning experiments (e.g. Schmitt et al., 1989; Capobianco et al., 1999). For In the data are in best agreement with a 1^+ valence. Not shown in the diagrams are Cr, Ni and Co, for which we derive 2^+ states and Ti, which seems to be intermediate between 3^+ and 2^+ possibly due to a mixture of these valence states in the melt. These valence states are also in good agreement with the higher pressure and temperature data. In Fig. A1, for example, trends for V and Nb at 6 GPa, 2373 K and 18 GPa, 2573 K are shown to be in good agreement with those determined at 2 GPa.

APPENDIX 3. THE EFFECT OF CARBON IN METALLIC ALLOYS

The metal–silicate partitioning of certain elements is strongly influenced by the solution of light elements, such as S, Si and C, in metallic Fe-liquids. These effects only become a problem, however, when light element concentrations are significantly greater in the experiments compared to realistic core fractionation scenarios. When graphite capsules are employed, for example, 1–9 wt% C dissolves in the metallic alloy, which is probably unrealistic for core formation and must be corrected for if data between different capsule types are to be compared.

In this study, C contents in metallic liquids were estimated from the deviation of totals of microprobe analyses from 100 wt%. Although only qualitative, the results compare well with trends derived from thermodynamic models (e.g. Bouchard and Bale, 1995) and with other studies (Corgne et al., 2008; Dasgupta and Walker, 2008) where more thorough analyses have been performed (Fig. A2). As seen in Fig. A2, the carbon content of the metal is inversely coupled to the Si content and consequently postively to fo_2, which is the result of the mutual avoidance of C and Si in metallic Fe-liquids. The effect of dissolved carbon on element partition coefficients can be corrected using previously described methods and literature data (Wade and Wood, 2005; Corgne et al., 2008). Where literature data were in poor agreement with our result, however, thermodynamic parameters were refined by comparing results from experiments performed using both MgO and graphite capsules at the same conditions. Dissolved C effects D_M through the activity coefficient γ_M^{metal} (see Eqs. (A10) and (A11)) and the oxygen fugacity through γ_{Fe}^{metal} (Eq. (A5)). If the magnitude of the change in γ_M^{metal} can be quantified for a given C content, then the C-free partition coefficient can be determined from the C-bearing value by simply adding a correction term, $\log \gamma_{M,cor}^{metal}$, to Eq. (A12) where:

$$\log \gamma_{M,cor}^{metal} = \log \gamma_{M,C=x}^{metal} - \log \gamma_{M,C=0}^{metal} \quad \text{(A13)}$$

Table A1
Metal–silicate partition coefficients D calculated on mol% basis.

Run	Si	±	Fe	±	Ti	±	V	±	Cr	±	Mn	±	Ta	±	Nb	±	Ga	±	In	±	Zn	±
P1-19[a]	0.11	0.01	270.8	65.4	0.09	0.07	—	—	19.64	7.93	0.48	0.11	4.96	2.47	—	—	77.40	97.77	11.00	2.24	5.80	0.40
P1-21[a]	0.01	0.00	85.93	20.56	0.03	0.04	—	—	7.08	2.01	0.09	0.08	0.39	0.13	—	—	20.21	20.70	6.63	1.67	1.35	0.47
P1-20[a]	0.00	0.00	13.96	0.94	0.02	0.04	—	—	0.73	0.29	0.01	0.02	0.00	0.01	—	—	6.31	2.57	4.44	1.19	0.20	0.06
CDF1-5	0.17	0.02	115.9	17.0	0.07	0.07	—	—	3.17	0.74	0.09	0.04	0.56	0.19	—	—	190.0	311.1	57.26	11.12	6.65	1.30
C15-9	0.10	0.01	89.54	2.76	0.00	0.00	1.70	0.03	2.42	0.16	0.10	0.01	0.07	0.02	2.27	0.48	—	—	—	—	—	—
CDF1-2	0.06	0.01	61.76	4.29	0.02	0.03	—	—	1.64	0.32	0.03	0.03	0.15	0.06	—	—	112.5	182.6	67.14	13.24	4.23	0.49
C15-10	0.01	0.00	36.71	2.50	0.00	0.00	0.45	0.04	0.96	0.12	0.03	0.01	0.01	0.01	0.25	0.06	—	—	—	—	—	—
CDF1-3	—	—	14.11	1.58	—	—	—	—	0.21	0.05	0.00	0.00	0.01	0.01	—	—	31.14	18.84	43.29	10.84	0.78	0.17
CDF1-4	—	—	11.11	2.40	0.02	0.05	—	—	0.15	0.05	—	—	0.05	0.12	—	—	20.51	15.97	43.08	17.33	0.53	0.13
CDF1-1[b]	0.00	0.00	12.99	2.95	0.02	0.03	2.20	1.00	1.50	0.67	0.12	0.04	0.02	0.05	0.03	0.03	3.48	2.10	55.87	37.08	0.49	0.73
V307[a]	0.40	0.02	339.7	175.5	0.38	0.48	—	—	30.74	28.24	0.35	0.50	31.83	49.88	—	—	39.76	13.69	10.99	9.23	4.80	1.36
V312[a]	0.09	0.01	90.61	33.06	0.07	0.08	—	—	5.61	4.29	0.16	0.49	1.60	0.71	—	—	16.00	4.24	8.07	2.91	2.18	0.35
V334[a]	0.01	0.01	43.25	5.46	0.02	0.01	4.55	1.28	5.88	1.51	0.22	0.04	0.28	0.38	8.24	12.41	—	—	—	—	—	—
V310[a]	0.01	0.00	27.01	1.98	0.04	0.06	—	—	3.48	0.93	0.14	0.14	0.12	0.03	—	—	8.30	1.65	5.46	1.36	0.53	0.11
V337[a]	—	—	15.97	0.63	0.01	0.00	1.07	0.17	2.09	0.36	0.10	0.02	0.01	0.01	0.41	0.27	—	—	—	—	—	—
V309[a]	0.00	0.00	7.98	1.18	0.02	0.03	—	—	1.33	4.50	0.09	0.31	0.00	0.01	—	—	1.21	1.01	1.43	0.84	0.19	0.33
V311[a]	0.00	0.00	7.55	0.93	0.02	0.04	—	—	0.55	0.21	0.01	0.05	0.01	0.01	—	—	0.89	0.65	1.36	0.88	0.08	0.04
V346	0.09	0.01	131.2	84.9	0.01	0.01	2.14	1.66	5.75	4.76	0.67	0.46	0.05	0.06	1.10	1.30	—	—	—	—	—	—
V366	0.09	0.00	104.3	16.1	0.01	0.00	2.22	0.30	5.49	0.86	0.66	0.09	0.09	0.04	1.58	0.65	—	—	—	—	—	—
V365	0.02	0.00	51.96	4.72	0.00	0.00	0.92	0.14	2.84	0.21	0.27	0.03	0.01	0.01	0.28	0.25	—	—	—	—	—	—
V367	0.11	0.00	93.31	12.22	0.01	0.00	2.20	0.27	5.57	0.50	0.82	0.08	0.11	0.06	1.65	0.96	—	—	—	—	—	—
V397[b]	0.05	0.02	55.90	10.23	0.15	0.22	8.35	1.97	4.71	1.07	0.92	0.50	0.36	0.16	8.48	3.37	48.76	41.91	142.2	41.4	4.11	0.95
Z457	0.01	0.00	13.71	0.61	0.02	0.03	—	—	0.52	0.11	0.03	0.07	0.00	0.01	—	—	8.76	1.50	7.62	3.21	0.77	0.07
Z442	0.21	0.03	57.60	5.82	0.04	0.03	—	—	3.84	0.56	0.74	0.20	0.40	0.27	—	—	52.68	42.44	19.95	4.25	2.49	0.22
Z469	0.16	0.02	39.83	7.77	0.01	0.01	0.61	0.24	2.45	0.57	0.59	0.21	0.06	0.09	0.71	1.18	—	—	—	—	—	—
Z474	0.07	0.03	23.57	9.86	0.01	0.01	0.32	0.15	1.37	0.56	0.30	0.13	0.01	0.02	0.29	0.39	—	—	—	—	—	—
Z448	0.23	0.01	49.34	5.40	0.02	0.03	—	—	3.94	0.50	0.91	0.19	0.14	0.06	—	—	36.96	20.31	15.99	2.43	3.21	0.23
Z551[b]	0.06	0.01	39.53	2.87	0.00	0.00	0.96	0.05	3.02	0.17	0.61	0.07	0.09	0.03	1.40	0.38	—	—	—	—	—	—
H2333[a]	0.13	0.02	111.1	49.1	0.22	0.07	—	—	54.86	9.07	3.65	1.03	4.48	4.21	—	—	23.64	5.07	3.94	3.24	1.17	0.46
H2340[a]	0.00	0.00	24.34	8.97	0.03	0.06	—	—	9.88	1.50	0.60	0.23	0.06	0.05	—	—	2.48	2.23	0.68	1.80	0.21	0.30
H2347[a]	0.00	0.00	11.57	0.96	0.02	0.05	—	—	2.01	0.47	0.18	0.11	0.00	0.00	—	—	0.66	0.47	0.27	0.72	0.06	0.08
H2350[a]	0.00	0.00	7.41	0.50	0.01	0.01	—	—	0.89	0.23	0.03	0.11	0.00	0.00	—	—	0.40	0.24	0.17	0.34	0.04	0.07
S3658	0.22	0.04	46.72	8.93	0.01	0.02	—	—	2.39	1.06	0.96	0.27	0.12	0.10	—	—	22.92	11.53	12.59	2.24	1.96	0.41

± Uncertainties determined from error propagation for the calculation of D from the standard deviations of the metal and the silicate concentration.

[a] Results from graphite capsules.

[b] Metal contains sulphur.

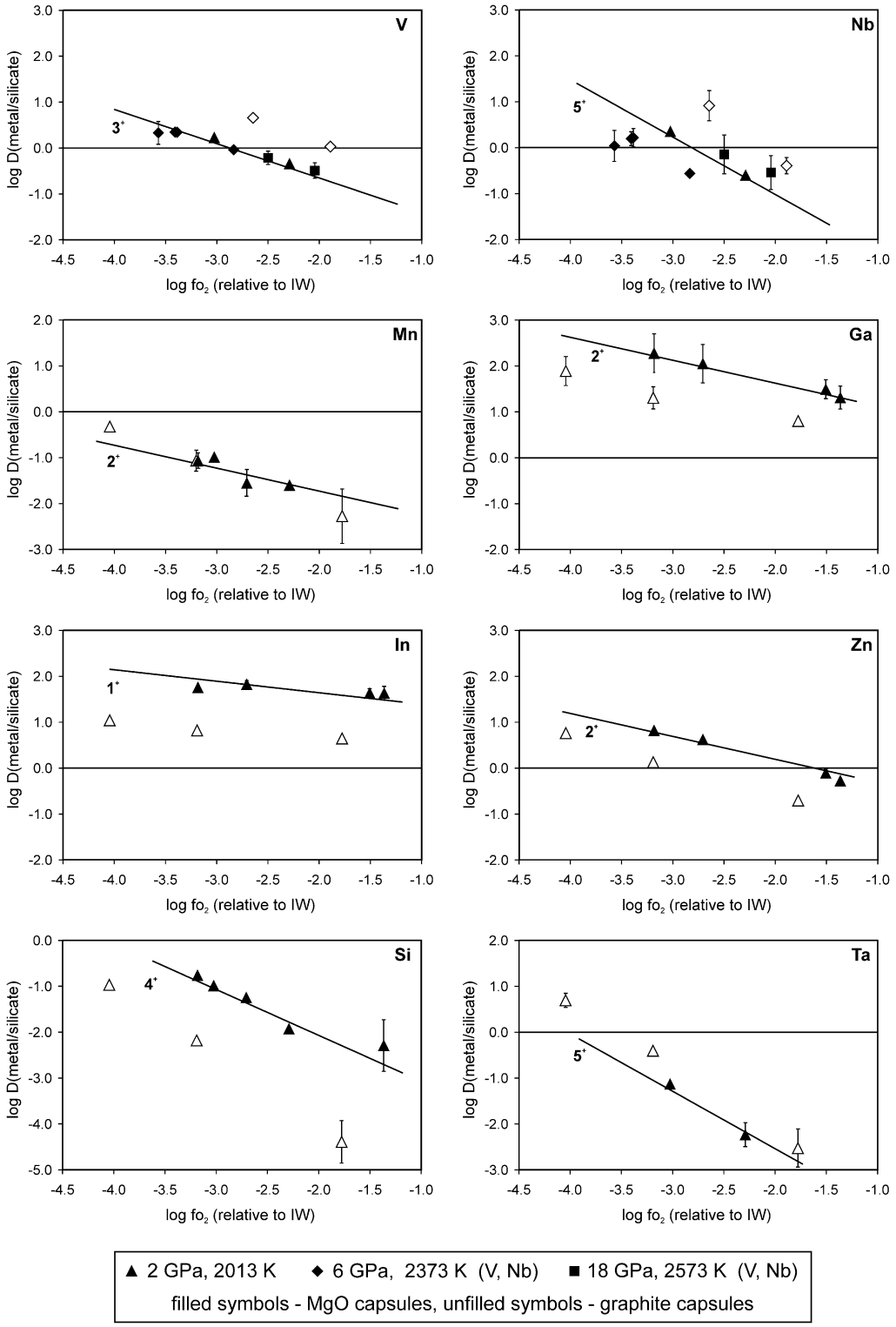

Fig. A1. Metal–silicate partition coefficients D (mol% basis) of S-free samples for V, Nb, Mn, Ga, In, Zn, Si and Ta plotted as a function of oxygen fugacity relative to the iron-wüstite buffer (ΔIW), as logarithmic values. Where no error bars are shown the uncertainties do not exceed the symbol size. Isobaric (2 GPa) and isothermal (~2023 K) results show the influence of the capsule material on the partition coefficients for Si, Ta, Mn, Ga, In, Zn. Results from MgO single-crystal capsules (black symbols) served as reference for results from graphite capsules (unfilled symbols) where C got dissolved in the metal liquids. The lines indicate the ideal valence (n^+) trend most likely for the respective element that is consistent with the data sets (see Appendix Eq. (A12)). For V and Nb graphite capsules were only employed for runs at 6 GPa, 2373 K. As we have only few data at 6 GPa for these two elements, results from various conditions are included in the respective diagrams in order to illustrate their valence trends.

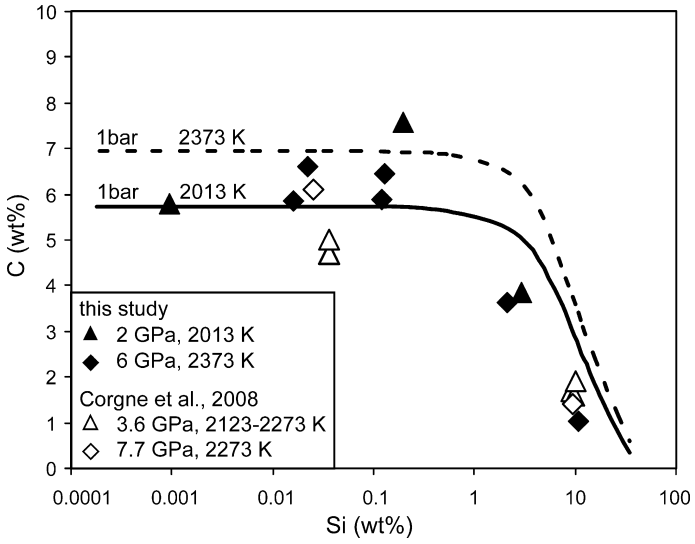

Fig. A2. Influence of Si on the concentration of C in liquid iron alloys. Experimental data at high pressure from this study and Corgne et al. (2008). In the latter study C contents in metallic liquids were analyzed, whereas in this study they were estimated from the deviation of totals of EPMA from 100 wt%. Trends at 1 bar are derived from the thermodynamic model of Bouchard and Bale (1995).

The correction is therefore the difference between the activity coefficient of an element in C-free metal and the one at the C content of interest at the same conditions.

As shown in previous studies (Wade and Wood, 2005; Corgne et al., 2008) a rigorous model for describing the effect of interacting solutes on each other's activity coefficients in Fe-alloys is given by Ma (2001). To correct for the C content we have employed the thermodynamically-consistent equation of Ma (2001) for the Fe–M–C ternary system (M = solute of interest) in conjunction with Eq. (A13) to determine log $\gamma^{metal}_{M,cor}$. Such equations involve several interaction parameters ε that take account of the mutual influence of the solutes M and C in the Fe liquid. However, in the course of our calculation, all interaction terms aside from those containing ε^C_M cancel out or play a negligible role. Values of ε^C_M can be found in the Steelmaking Data Sourcebook (SDS) and are listed for the elements of interest in Table A2 along with typical correction values log $\gamma^{metal}_{M,cor}$ that we employed. Where the corrections were in good agreement with the differences in log D found between graphite and MgO capsule experiments, the SDS ε^C_M values were preferred. Using results of experiments from both capsule types, however, we refined values for Ta, Nb, Cr and Mn because results deviated significantly from the SDS data and values for Ga, In, Zn and Ti have not been previously reported (Table A2). We note that errors in determined C contents of 2 wt% propagate in most cases to errors in the corrected log D values of less than 0.3 log units, but for elements with large absolute ε^C_M values (especially those with negative values) like V, Ta, Nb or In and Si, this increases to 0.4–0.6 log units, underlining the importance of accurate C content determination if the partitioning of these elements is to be studied using graphite capsules.

Table A2
Interaction parameters ε[a] between carbon and solutes M in liquid Fe-alloy and the resulting metal activity coefficient (γ) correction term for D in C-bearing samples (based on Ma, 2001; see Appendix).

M	ε^C_M SDS[b] (1873 K)	ε^C_M this study (1873 K)	log $\gamma^{metal}_{M,cor}$ [c] (2000 K)
Si	9.68		0.95
Ta	—168.5	−4.26	−0.70
Nb	—22.72	−2.60	−0.50
V	−5.95		−0.86
Cr	−4.85	−1.74	−0.40
Mn	−1.87	2.02	0.04
Ga		8.68	0.82
In		11.90	1.20
Zn		7.24	0.66
Ti		−4.31	−0.70

[a] ε^C_M values based on mol fraction.
[b] SDS, Steelmaking Data Sourcebook.
[c] Calculated for $X_C = 0.25$.

The effect of C is consistent with trends observed for the partitioning behaviour of V and Cr reported by Chabot and Agee (2003). The importance of accounting for this effect is emphasised in Fig. A1. If results from graphite capsules are employed without corrections, an element such as Si would appear significantly more lithophile than Ta, whereas in fact they have very similar lithophile tendencies.

REFERENCES

Barin I., Sauert F., Schultze-Rhonhof E. and Sheng W. S. (1989) *Thermochemical Data of Pure Substances, Part I and Part II*. Verlagsgesellschaft Weinheim, Germany, pp. 1739.

Bouchard D. and Bale C. W. (1995) Simultaneous-optimization of thermochemical data for liquid-iron alloys containing C, N, Ti, Si, Mn, S, and P. *Metall. Mater. Trans. B Proc. Metal. Mater. Proc. Sci.* **26**, 467–484.

Capobianco C. J., Drake M. J. and de'Aro J. (1999) Siderophile geochemistry of Ga, Ge, and Sn: cationic oxidation states in silicate melts and the effect of composition in iron–nickel alloys. *Geochim. Cosmochim. Acta* **63**, 2667–2677.

Chabot N. L. and Agee C. B. (2003) Core formation in the Earth and Moon: new experimental constraints from V, Cr, and Mn. *Geochim. Cosmochim. Acta* **67**, 2077–2091.

Chabot N. L., Draper D. S. and Agee C. B. (2005) Conditions of core formation in the earth: constraints from Nickel and Cobalt partitioning. *Geochim. Cosmochim. Acta* **69**, 2141–2151.

Chase M. W., Davies C. A., Downey J. R., Frurip D. J., McDonald R. A. and Syverud A. N. (1998) *NIST — JANAF Thermochemical Tables, fourth ed. Part 1 and Part 2, vol. 14 Monograph*. National Institute of Standards Technology.

Corgne A., Keshav S., Wood B. J., McDonough W. F. and Fei Y. W. (2008) Metal–silicate partitioning and constraints on core composition and oxygen fugacity during Earth accretion. *Geochim. Cosmochim. Acta* **72**, 574–589.

Dasgupta R. and Walker D. (2008) Carbon solubility in core melts in a shallow magma ocean environment and distribution of carbon between the Earth's core and the mantle. *Geochim. Cosmochim. Acta* **72**, 4627–4641.

Dreibus G. and Palme H. (1996) Cosmochemical constraints on the sulfur content in the Earth's core. *Geochim. Cosmochim. Acta* **60**, 1125–1130.

Frost D. J. (2003) Fe^{2+}–Mg partitioning between garnet, magnesiowustite, and $(Mg, Fe)_2SiO_4$ phases of the transition zone. *Am. Miner.* **88**, 387–397.

Gessmann C. K. and Rubie D. C. (1998) The effect of temperature on the partitioning of nickel, cobalt, manganese, chromium, and vanadium at 9 GPa and constraints on formation of the Earth's core. *Geochim. Cosmochim. Acta* **62**, 867–882.

Gessmann C. K. and Rubie D. C. (2000) The origin of the depletions of V, Cr and Mn in the mantles of the Earth and Moon. *Earth Planet. Sci. Lett.* **184**, 95–107.

Gessmann C. K., Rubie D. C. and McCammon C. A. (1999) Oxygen fugacity dependence of Ni, Co, Mn, Cr, V, and Si partitioning between liquid metal and magnesiowustite at 9–18 GPa and 2200 °C. *Geochim. Cosmochim. Acta* **63**, 1853–1863.

Gessmann C. K., Wood B. J., Rubie D. C. and Kilburn M. R. (2001) Solubility of silicon in liquid metal at high pressure: implications for the composition of the Earth's core. *Earth Planet. Sci. Lett.* **184**, 367–376.

Herzberg C. and Zhang J. Z. (1996) Melting experiments on anhydrous peridotite KLB-1: compositions of magmas in the upper mantle and transition zone. *J. Geophys. Res. Solid Earth* **101**, 8271–8295.

Hillgren V. J., Drake M. J. and Rubie D. C. (1996) High pressure and high temperature metal–silicate partitioning of siderophile elements: the importance of silicate liquid composition. *Geochim. Cosmochim. Acta* **60**, 2257–2263.

Humayun M. and Cassen P. (2000) Processes determining the volatile abundances of meteorites and the terrestrial planets. In *Origin of the Earth and Moon* (eds. R. M. Canup and K. Righter). The University of Arizona Space Science Series, pp. 3–23.

Ito E., Morooka K., Ujike O. and Katsura T. (1995) Reactions between molten iron and silicate melts at high-pressure — implications for the chemical evolution of Earths core. *J. Geophys. Res. Solid Earth* **100**, 5901–5910.

Ito E., Kubo A., Katsura T. and Walter M. J. (2004) Melting experiments of mantle materials under lower mantle conditions with implications for magma ocean differentiation. *Phys. Earth Planet. Inter.* **143–144**, 397–406.

Jaeger W. L. and Drake M. J. (2000) Metal–silicate partitioning of Co, Ga, and W: dependence on silicate melt composition. *Geochim. Cosmochim. Acta* **64**, 3887–3895.

Jana D. and Walker D. (1997) The influence of silicate melt composition on distribution of siderophile elements among metal and silicate liquids. *Earth Planet. Sci. Lett.* **150**, 463–472.

Kegler P., Holzheid A., Frost D. J., Rubie D. C., Dohmen R. and Palme H. (2008) New Ni and Co metal–silicate partitioning data and their relevance for an early terrestrial magma ocean. *Earth Planet. Sci. Lett.* **268**, 28–40.

Kilburn M. R. and Wood B. J. (1997) Metal–silicate partitioning and the incompatibility of S and Si during core formation. *Earth Planet. Sci. Lett.* **152**, 139–148.

Li J. and Agee C. B. (1996) Geochemistry of mantle — core differentiation at high pressure. *Nature* **381**, 686–689.

Li J. and Agee C. B. (2001) The effect of pressure, temperature, oxygen fugacity and composition on partitioning of nickel and cobalt between liquid Fe–Ni–S alloy and liquid silicate: implications for the earth's core formation. *Geochim. Cosmochim. Acta* **65**, 1821–1832.

Ma Z. T. (2001) Thermodynamic description for concentrated metallic solutions using interaction parameters. *Metall. Mater. Trans. B Proc. Metal. Mater. Proc. Sci.* **32**, 87–103.

Malavergne V., Siebert J., Guyot F., Gautron L., Combes R., Hammouda T., Borensztajn S., Frost D. and Martinez I. (2004) Si in the core? New high-pressure and high-temperature experimental data. *Geochim. Cosmochim. Acta* **68**, 4201–4211.

Malavergne V., Tarrida M. and Combes R., et al. (2007) New high-pressure and high-temperature metal/silicate partitioning of U and Pb: implications for the cores of the Earth and Mars. *Geochim. Cosmochim. Acta* **71**, 2637–2655.

McDonough W. F. and Sun S. (1995) The composition of the Earth. *Chem. Geol.* **120**, 223–253.

Münker C., Pfander J. A., Weyer S., Buchl A., Kleine T. and Mezger K. (2003) Evolution of planetary cores and the earth–moon system from Nb/Ta systematics. *Science* **301**, 84–87.

Newsom H. E. (1990) Accretion and core formation in the Earth: evidence from Siderophile elements. In *Origin of the Earth* (eds. H. E. Newsom and J. H. Jones). Oxford University Press, New York.

Ohtani E., Yurimoto H. and Seto S. (1997) Element partitioning between metallic liquid, silicate liquid, and lower-mantle minerals: implications for core formation of the Earth. *Phys. Earth Planet. Inter.* **100**, 97–114.

O'Neill H. S. C. (1991) The origin of the moon and the early history of the Earth — a chemical model. Part 2: the Earth. *Geochim. Cosmochim. Acta* **55**, 1159–1172.

O'Neill H. S. C. and Eggins S. M. (2002) The effect of melt composition on trace element partitioning: an experimental investigation of the activity coefficients of FeO, NiO, CoO, MoO_2 and MoO_3 in silicate melts. *Chem. Geol.* **186**, 151–181.

O'Neill H. S. C. and Palme H. (1998) Composition of the silicate Earth; implications for accretion and core formation. In *The Earth's Mantle; Composition, Structure, and Evolution* (ed. I. Jackson). Cambridge University Press, pp. 3–126.

O'Neill H. S. C. and Palme H. (2008) Collisional erosion and the non-chondritic composition of the terrestrial planets. *Phil. Trans. R. Soc. A* **366**, 4205–4238.

O'Neill H. S. C., Canil D. and Rubie D. C. (1998) Oxide–metal equilibria to 2500 °C and 25 GPa: implications for core formation and the light component in the Earth's core. *J. Geophys. Res.* **103**, 12239–12260.

Palme H. and O'Neill H. S. C. (2003) Cosmochemical estimates of mantle composition. In *Treatise on Geochemistry. The Mantle and Core*, vol. 2 (ed. H. D. Holland). Elsevier Pergamon, Oxford, pp. 1–38.

Rammensee W., Palme H. and Wänke H. (1983) Experimental investigation of metal-silicate partitioning of some lithophile elements (Ta, Mn, V, Cr). *Lunar Planet. Sci. XIV*. Lunar Planet. Inst., Houston. pp. 628–629 (abstr.).

Righter K. and Drake M. J. (2000) Metal/silicate equilibrium in the early Earth — new constraints from the volatile moderately

siderophile elements Ga, Cu, P, and Sn. *Geochim. Cosmochim. Acta* **64**, 3581–3597.

Righter K. and Drake M. J. (2003) Partition coefficients at high pressure and temperature. In *Treatise on Geochemistry. The Mantle and Core*, vol. 2 (ed. H. D. Holland). Elsevier Pergamon, Oxford, pp. 425–449.

Righter K., Drake M. J. and Yaxley G. (1997) Prediction of siderophile element metal–silicate partition coefficients to 20 GPa and 2800 °C: the effects of pressure, temperature, oxygen fugacity, and silicate and metallic melt compositions. *Phys. Earth Planet. Inter.* **100**, 115–134.

Ringwood A. E. (1979) *Origin of the Earth and Moon*. Springer Verlag, Berlin.

Rubie D. C. (1999) Characterising the sample environment in multi-anvil high-pressure experiments. *Phase Transitions* **68**, 431–451.

Rubie D. C., Melosh H. J., Reid J. E., Liebske C. and Righter K. (2003) Mechanisms of metal–silicate equilibration in the terrestrial magma ocean. *Earth Planet. Sci. Lett.* **205**, 239–255.

Rubie D. C. and Frost D. J. (2007) New constraints on conditions of core formation and the light element content of the Earth's core. *Geochim. Cosmochim. Acta* **71**, A857 (abstr.).

Rubie D. C., Nimmo F. and Melosh H. J. (2007) Formation of the Earth's core. In *Treatise on Geophysics. Evolution of the Earth*, vol. 9 (ed. D. J. Stevenson). Elsevier, Amsterdam, pp. 51–90.

Rudnick R. L., Barth M., Horn I. and McDonough W. F. (2000) Rutile — bearing refractory eclogites: missing link between continents and depleted mantle. *Science* **287**, 278–281.

Schmitt W., Palme H. and Wänke H. (1989) Experimental determination of metal/silicate partition coefficients for P, Co, Ni, Cu, Ga, Ge, Mo and W and some implications for the early evolution of the Earth. *Geochim. Cosmochim. Acta* **53**, 173–185.

Takafuji N., Hirose K., Mitome M. and Bando Y. (2005) Solubilities of O and Si in liquid iron in equilibrium with $(Mg,Fe)SiO_3$ perovskite and the light elements in the core. *Geophys. Res. Lett.* **32**, 6313. doi:10.1029/2005GL022773.

The Japan Society for the Promotion of Science and The Nineteenth Committee on Steelmaking (1988) *Steelmaking Data Source Book*. Gordon and Breach Science Publishers, Montreux.

Thibault Y. and Walter M. J. (1995) The influence of pressure and temperature on the metal–silicate partition-coefficients of nickel and cobalt in a model-CI chondrite and implications for metal segregation in a deep magma ocean. *Geochim. Cosmochim. Acta* **59**, 991–1002.

Trønnes R. G. a. F. and Frost D. J. (2002) Peridotite melting and mineral–melt partitioning of major and minor elements at 22–24.5 GPa. *Earth Planet. Sci. Lett.* **197**, 117–131.

Wade J. and Wood B. J. (2001) The Earth's 'missing' niobium may be in the core. *Nature* **409**, 75–78.

Wade J. and Wood B. J. (2005) Core formation and the oxidation state of the Earth. *Earth Planet. Sci. Lett.* **236**, 78–95.

Walter M. J., Newsom H. E., Ertel W. and Holzheid A. (2000) Siderophile elements in the earth and moon: metal/silicate partitioning and implications for core formation. In *Origin of the Earth and Moon* (eds. R. M. Canup and K. Righter). The University of Arizona Space Science Series, pp. 265–289.

Wänke H. (1981) Constitution of terrestrial planets. *Phil. Trans. R. Soc.* **303**, 287–302.

Wasson J. T. (1985) *Meteorites their Record of Early Solar-system History*. Freeman, New York, pp. 267.

Wasson J. T. and Kallemeyn G. W. (1988) Compositions of chondrites. *Phil. Trans. R. Soc. A* **325**, 535–544.

Wheeler K. T., Walker D., Fei Y. W., Minarik W. G. and McDonough W. F. (2006) Experimental partitioning of uranium between liquid iron sulfide and liquid silicate: implications for radioactivity in the Earth's core. *Geochim. Cosmochim. Acta* **70**, 1537–1547.

Wood B. J., Nielsen S. G., Rehkämper M. and Halliday A. N. (2008a) The effects of core formation on the Pb- and Tl-isotopic composition of the silicate Earth. *Earth Planet. Sci. Lett.* **269**, 326–336.

Wood B. J., Wade J. and Kilburn M. R. (2008b) Core formation and the oxidation state of the Earth: additional constraints from Nb, V and Cr partitioning. *Geochim. Cosmochim. Acta* **72**, 1415–1426.

Yi W., Halliday A. N., Alt J. C., Lee D.-Ch., Rehkämper M., Garcia M. and Su Y. (2000) Cadmium, indium, tin, tellurium, and sulfur in oceanic basalts; implications for chalcophile element fractionation in the Earth. *J. Geophys. Res. B Solid Earth Planets* **105**, 18927–18948.

Zerr A., Diegeler A. and Boehler R. (1998) Solidus of Earth's deep mantle. *Science* **281**, 243–246.

Associate editor: Richard J. Walker